5-9-2015

Electrostatic Interactions Stabilizing the I-domain of Bacteriophage P22

Christina Harprecht
University of Connecticut - Storrs, christina.harprecht@uconn.edu

Electrostatic Interactions Stabilizing the I-domain of Bacteriophage P22

Christina Harprecht

B.S., Heinrich-Heine Universität Düsseldorf, 2012

A Thesis

Submitted in Partial Fulfillment of the

Requirements for the Degree of

Master of Science

At the

University of Connecticut

2015

APPROVAL PAGE

Masters of Science Thesis

Electrostatic Interactions Stabilizing the I-domain of Bacteriophage P22

Presented by

Christina Harprecht, B.S.

Major Advisor_____
Dr. Andrei T. Alexandrescu

Associate Advisor_____
Dr. Carolyn M. Teschke

Associate Advisor_____
Dr. Victoria L. Robinson

University of Connecticut

2015

Acknowledgements

I would like to thank my advisor, Andrei Alexandrescu, for his help and expertise during the past two years.

I would like to thank Carol Teschke for letting me work on this project and her help and guidance.

I would like to thank the current and former lab members from both labs.

Contents

Abstract v

Chapter 1: Introduction to P22 and the I-domain 1

Chapter 2: pH-titration of the I-domain via Nuclear Magnetic Resonance Spectroscopy 7

pH titrations of acidic residues in the P22 I-domain 7

pH titration of His_6 tag and His305 12

Chapter 3: Urea Denaturation Experiments 17

Urea Equilibrium Denaturation Experiments of D302A and H305A I-domain 17

Determination of melting transition of H305A and D302A I-domain via Circular Dichroism 24

Chapter 4: Hydrogen-Deuterium-Exchange Experiments 26

Hydrogen Exchange experiments of H305A and D302A via NMR 26

Chapter 5: Conclusions, Discussion & Future Work 36

Chapter 6: Materials and Methods 39

H305A and D302A I-domain expression and purification 39

NMR spectroscopy 40

pH titration of I-domain and Histidines 40

pH titration of acidic residues in the I-domain 41

Hydrogen-Deuterium Exchange Experiments 41

Circular Dichroism 42

Urea Denaturation 42

Melting Transition 42

Table of Figures 43

Bibliography 44

Abstract

The non-conserved I-domain of bacteriophage P22, a 123 residue part of the coat protein, plays an important role in folding and stability of viral capsids. In this study, the electrostatic interactions within the I-domain were investigated in order to determine which residues contribute to the overall stability of the I-domain. Out of 11 acidic residues within the I-domain, 8 are involved in electrostatic interactions according to their apparent pK_a value, which was determined in NMR pH-titration experiments. In particular, this study concentrates on the salt-bridge between H305 and D302. Two single amino acid variants, H305A and D302A, were created and their influences on the stability of the I-domain investigated. The thermodynamic stability of the H305A and D302A I-domain as a function of denaturant was determined using circular dichroism spectroscopy. In these experiments, the ΔG_0 for H305A was determined to be 6.0 kcal/mol at pH 6.5, which is nearly the same like the one for WT I-domain (6.2 kcal/mol). ΔG_0 for D302A is significantly lower at 3.3 kcal/mol. The stability of the I-domain has been further investigated by NMR Hydrogen-Deuterium (HX) exchange experiments. Here, amide protons of the D302A I-domain exchanged significantly faster than the amide protons of H305A, which showed exchange rates similar to WT I-domain. The ΔG_0 values determined by HX experiments were 6.3 kcal/mol and 4.3 kcal/mol for H305A and D302A, respectively. WT I-domain shows a significantly higher ΔG_0 value of 8.3 kcal/mol for NMR HX experiments compared to the ΔG_0 value determined via CD. In the structure of the I-domain, β-strands showed increased stability against exchange unlike the single α-helix, which seems not to be protected. Taken together, the urea equilibrium denaturation and HX experiments indicate a significantly lower stability for D302A than for H305A.

Chapter 1

Introduction to P22 and the I-domain

Bacteriophage P22, which infects *Salmonella enterica* serovar Typhimurium, has long been a model used for understanding assembly mechanisms of double-stranded DNA (dsDNA) viruses (1), including human viruses such as herpes simplex virus type 1 (HSV-1). In the assembly of P22, 415 copies of coat protein interact with 60-300 copies of scaffolding protein, which is known to be a chaperone for procapsid assembly. In this nucleation-limited reaction, 12 copies of portal protein (gp1) and 12-20 copies of multiple ejection proteins (gp7, gp16 and gp20) are added to form the procapsid (2). The coat protein shell of P22 procapsids is composed of the dodecameric portal complex and 71 capsomers, icosahedral subunits of the capsid, of which 60 are hexons and 11 are pentons (3) (see Figure 1). The maturation of procapsids into virions is continued by the packaging of the dsDNA genome through the portal complex with concomitant release of scaffolding protein (4). In the final maturation steps the virus head increases in its volume (5) and the tail spike proteins (gp9) are added to the virus head (6) to form the infectious virion.

Tailed dsDNA bacteriophages are the most abundant of all viruses in the biosphere. The coat proteins of prokaryote-infecting tailed DNA bacteriophages (*Caudovirales*) and eukaryote-infecting herpesviruses (*Herpesviridae*) adopt a common, HK97-like fold (7; 8). This HK97-like fold is essential for the assembly of the phage (3) and received its name from the first high-

resolution structure of this type of protein, the coat protein of the Hong Kong97 phage which infects *Escherichia coli* (8) (see Figure 3).

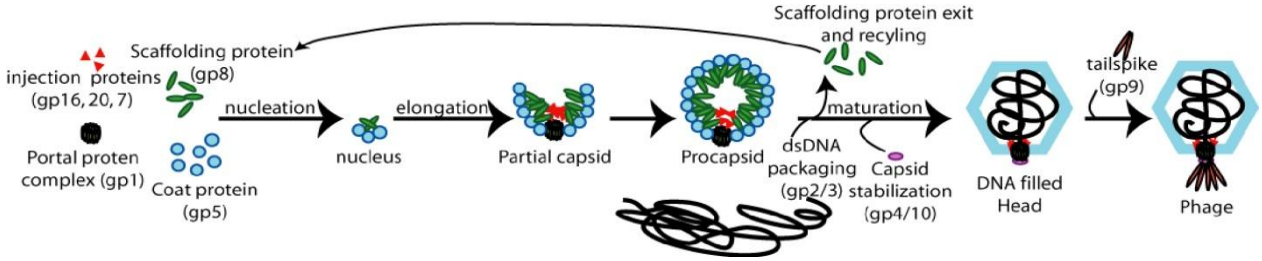

Figure 1: The assembly pathway of bacteriophage P22

This figure represents the assembly pathway of bacteriophage P22 like described in "Background" (modified from Teschke, Parent, 2010 (1))

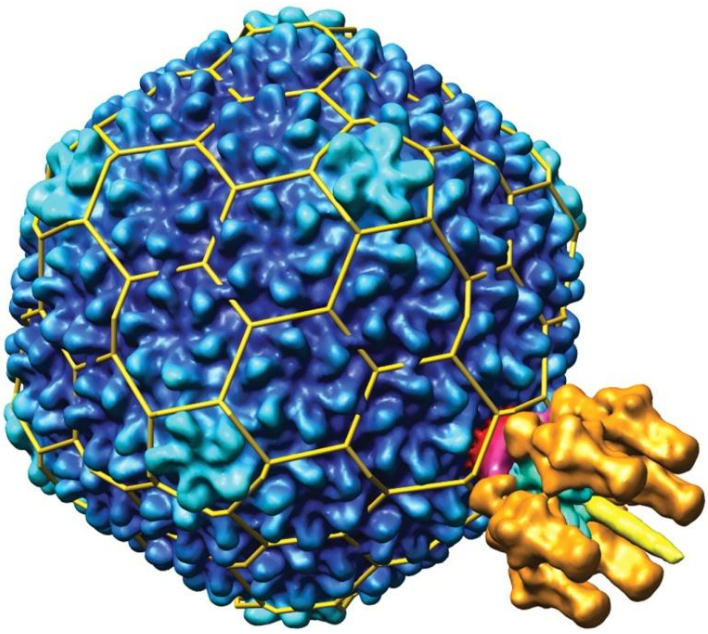

Figure 2: CryoEM reconstruction of P22 bacteriophage virion

The T=7 icosahedral symmetry of the coat protein shell is shown by the yellow lattice. Hexons are depicted in a darker blue and pentons in teal (modified from Lander et al., 2006 (9)).

Unlike bacteriophage P22, many viruses with the ubiquitous HK97-fold utilize host- or virus-encoded folding chaperones for the proper folding of their viral coat proteins. The coat protein of bacteriophage P22 is comprised of 430 amino acids and thereby contains 148 more residues than the coat protein of HK97 (10). Two independent studies of the P22 procapsid based on cryo-EM reconstructions have shown that the conserved HK97-fold forms the core of the coat protein structure (11; 3). These independent studies identified an additional domain, which was previously called the "telokin-like" (TL) domain according to Parent et al. or "extra-density" domain according to Chen et al., but is now called the "insertion" domain or I-domain (3; 11; 12). Different hypotheses were made about the structure and function of the I-domain. In the model of Chen et al. (2011) a loop region in the I-domain with overall positively charged residues called D-loop was suggested to make inter-capsomer contacts with adjacent coat protein monomers of the procapsid and mature virion (see Figure 4) and, therefore, was hypothesized to provide additional thermodynamic stability to the mature virion (11). The model of Parent et al. (2010) suggests the I-domain serves as the folding nucleus and contributes to the stability of the coat protein monomers (3). Its importance for the folding and stability of coat protein monomers is signified by *in-vivo* studies of temperature-sensitive-folding (*tsf*) amino acid substitutions in the coat protein (1) (13). Temperature-sensitive-folding mutants are able to make phage at permissive temperatures but cause the coat protein to aggregate at nonpermissive temperatures (14). The majority of known *tsf* substitutions are localized in the I-domain, implying it has a role in stabilization and folding of coat protein monomers (15). Chen et al. solved the structure of the coat protein of P22 to a resolution of 3.8 Å (11) whereas Parent et al. obtained reconstructions of cryoEM data at a resolution of 8.2 Å

(3). These models showed marked differences, one such difference involved residues 257 to 277, that in the model of Chen et al. were modeled as a loop called the D-loop (11) while in the other model it formed a β-strand (3). Furthermore, residues 322 to 326 formed an α-helix in the model proposed by Chen et al. (11), while in the model of Parent et al. they did not (3). To resolve these differences and to find out more about the function and role of the I-domain in procapsid assembly and stability, it was crucial to obtain a high-resolution structure. In 2013, Rizzo et al. determined the solution structure of the I-domain by NMR, using a fragment of the intact P22 coat protein encompassing residues 223 to 345 (see Figure 5). This high-resolution structure shows some striking differences from both cryoEM models, although they all show a high β-sheet content. While Parent et al.'s model proposed that the I-domain adopts a telokin-like fold, which arranges in a β-sandwich, the NMR structure actually shows that the I-domain adopts a β-barrel fold with strands 1 and 6 closing the barrel, bringing the amino (N) and carboxy (C) termini in close proximity. The D-loop which was suggested to make intercapsomer contacts in the model of Chen et al. is part of a β-sheet region and the actual D-loop was shown to be at a different position in the protein sequence. While the cryoEM model showed an overall positive charge for the D-loop, the NMR structure revealed an overall negative charge with one basic (K249) and three acidic residues (D244, D246 and D253). The α-helix, which is present in both models, was found to be formed by residues P322 to Y327 instead of residues V278 to L289 (12; 11; 3).

Since the high-resolution structure of the I-domain of bacteriophage P22 was solved in 2013 it is now possible to determine residues which contribute to the overall stability and perform mutagenesis experiments which can help understanding the function of the I-domain.

These residues might even be conserved in other dsDNA bacteriophages and related, higher order, eukaryotic viruses.

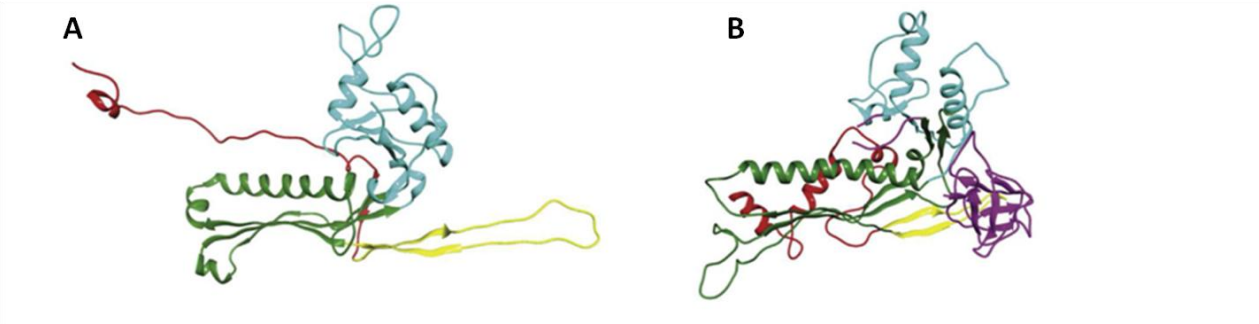

Figure 3: HK97 coat protein structure (A) and P22 coat protein structure (B) in comparison

A comparison of the coat protein cryoEM models of HK97 (in panel A) and P22 (panel B) show that the core of P22 adopts the HK97-like fold. Additionally, P22 contains the I-domain which is shown in magenta (B) (modified from Parent et al., 2010 (3)).

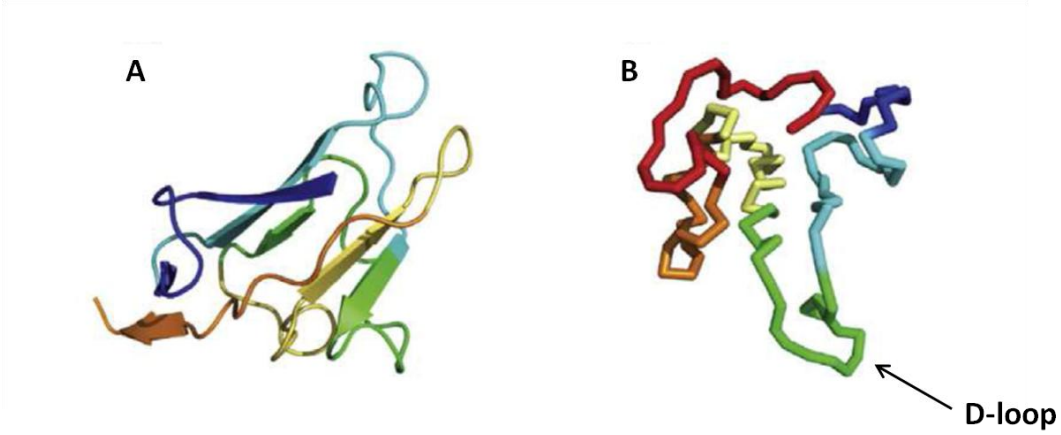

Figure 4: Comparison of the cryoEM models from Parent et al. (2010) and Chen et al.(2011)

Panel (A) shows a ribbon diagram of the I-domain structure from the 8.2 Å resolution cryoEM reconstruction of Parent et al. (2010). The coloring scheme is according to the residue position in the sequence with N-terminal residues in blue and C-terminal ones in red whereas residues 314 to 345 (red) could not be modeled using cryoEM data. Panel (B) depicts the model from the 3.8 Å resolution cryoEM reconstruction of Chen et al. (2011). Secondary structure elements are not identified in this model since it only has Cα atoms. The coloring scheme is identical to (B) (figure modified from Rizzo et al., Structure (2014) (12)) .

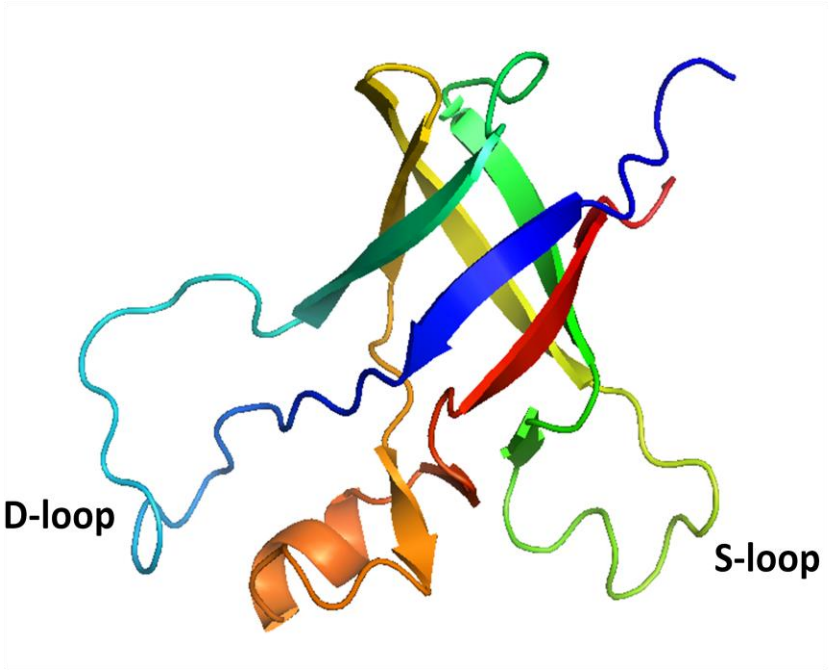

Figure 5: High resolution structure of the I-domain of bacteriophage P22

High resolution structure of the I-domain of bacteriophage P22. The coloring scheme is according to the protein sequence, starting at the N-terminus in blue changing to red at the C-terminus. (PDB entry 2M5S, modified from Rizzo et al., Structure (2014) (12))

Chapter 2

pH-titration of the I-domain via Nuclear Magnetic Resonance Spectroscopy

pH titrations of acidic residues in the P22 I-domain

The I-domain of the bacteriophage P22 contains 11 acidic residues nine of which are aspartates and two are glutamates (see Figure 6). Due to the fact that ionizable groups are important for the folding and the overall stability of a protein, pK_a values were determined for those residues. NMR has been shown to be a useful means for studying electrostatic interactions because pK_a values of ionizable groups can be monitored by following chemical shifts as a function of pH (16). In this study, the chemical shifts of the acidic residues of the I-domain were monitored to find out which of those residues could participate in salt-bridges and therefore might contribute to the overall stability of the I-domain. 2D ^{1}H-^{15}N-HSQC and 3D ^{1}H-^{15}N-NOESY-HSQC at different pH values were performed to investigate potential changes in chemical shifts caused by the gradual addition of acid or base. The 2D ^{1}H-^{15}N-HSQC provides a correlation between the nitrogen and amide proton so each amide results in one observable peak in the spectrum. Furthermore, 3D ^{1}H-^{15}N-NOESY-HSQC experiments show all proton resonances which are within 5 Å of the regarding amide proton (see Figure 7) and therefore can transfer magnetization from aspartate and glutamate side chains to the backbone HN, which have better dispersion (17). Chemical shifts were plotted as a function of pH and fitted to a modified Henderson-Hasselbalch equation to determine the pK_a (18).

$$\delta = \delta_{low} - \frac{\delta_{low} - \delta_{high}}{1 + 10^{n(pKa - pH)}}$$

Equation 1

Here, the pK_a (apparent ionization constant), δ_{low} (low pH chemical shift plateau), δ_{high} (high pH chemical shift plateau) and *n* (Hill coefficient, a measure of cooperativity) are the fitted variables in the plot of chemical shifts as a function of pH.

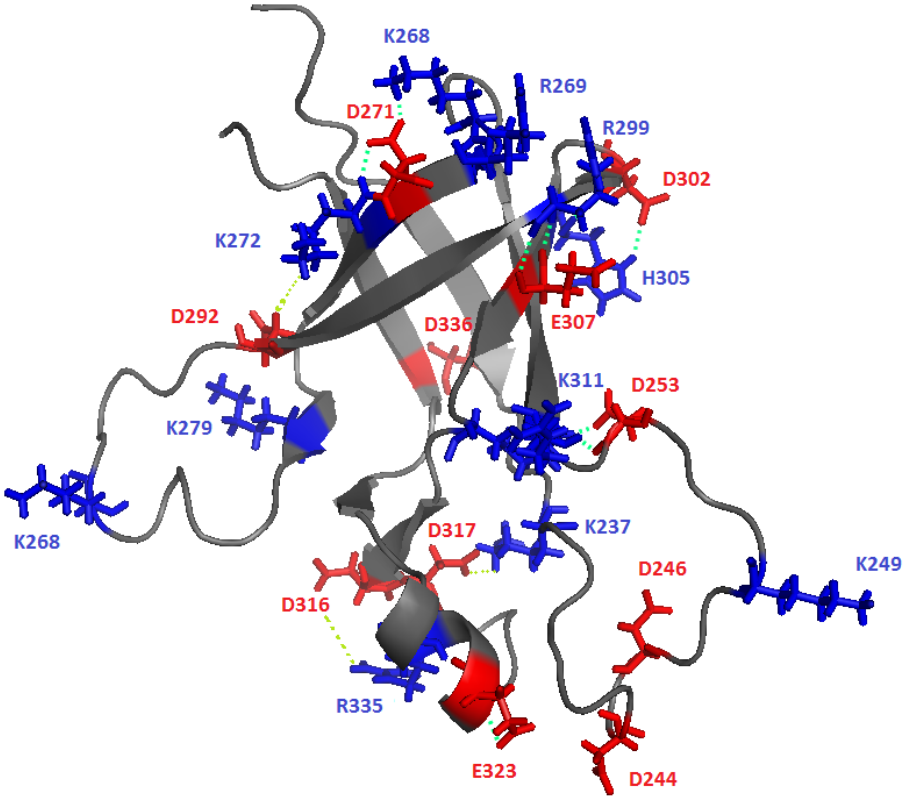

Figure 6: Structure of the I-domain of P22 with highlighted acidic residues

High resolution NMR structure shown in grey with highlighted and labeled acidic residues and basic residues represented as sticks. Aspartates and glutamates are colored in red, lysines, arginines and histidine are colored in blue in the ribbon diagram. Electrostatic interactions are shown as green dashes.

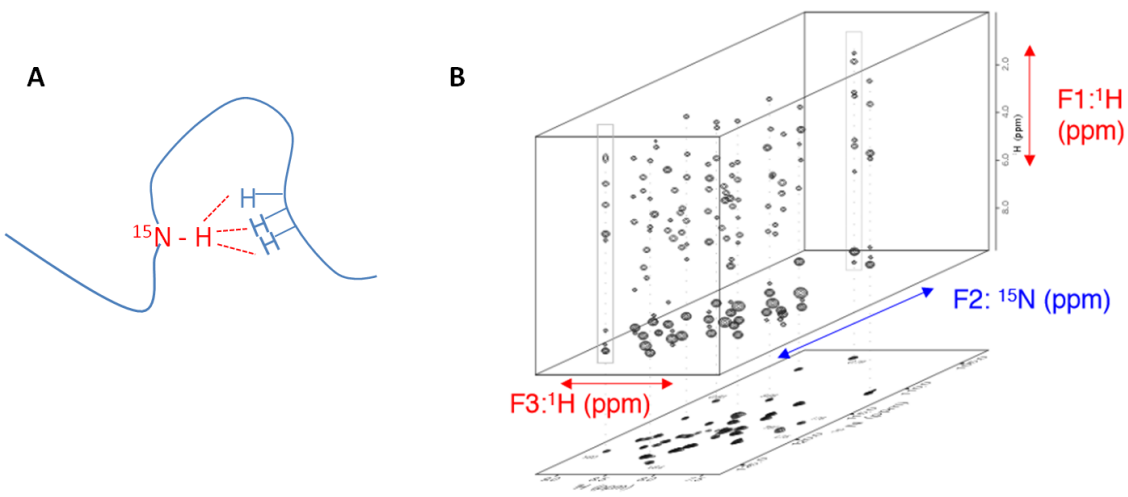

Figure 7: Schematic illustration of 3D ^{1}H-^{15}N NOESY-HSQC

Panel A represents the NOEs of amide protons to protons within 5 Å in the protein structure. Panel B exemplifies the different aspects of a 3D ^{1}H-^{15}N-NOESY-HSQC spectrum where plane F2/F3 depicts the 2D ^{1}H-^{15}N-HSQC correlation and plane F1/F3 depicts the proton correlation of 2D ^{1}H-^{1}H-NOESY

H305 and D302 are most likely interacting via a salt bridge

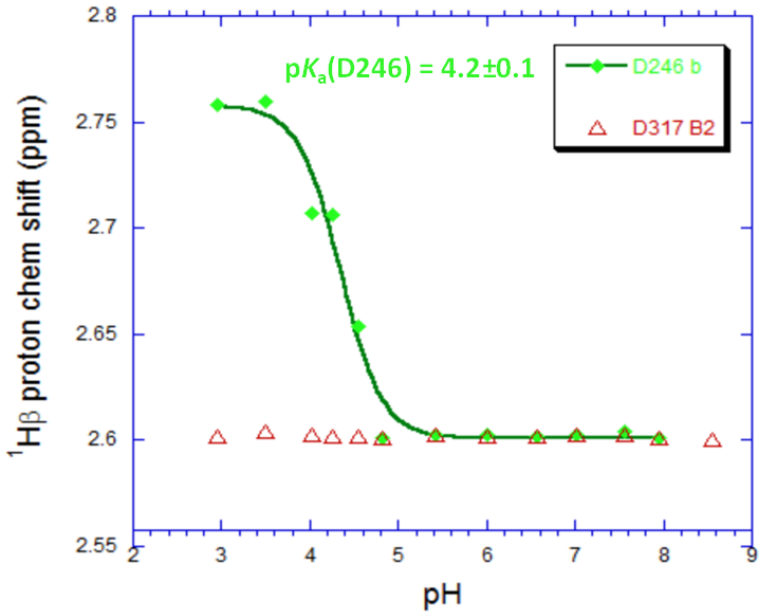

Figure 8: Representative pH titration data showing residues Aspartate at position 246 and 317

Asp317 is representing a non-shifting residue, whereas Asp 246 represents a shifting residue. The titration curves of the shifting residues were fit to a modified Henderson-Hasselbalch equation (see Equation 1). The pKa values from the fits are given in Table 1.

Table 1: Summary of pH-titratable acidic residues in and their corresponding pKa values

Residue	pKa	Energetics of shift	Salt bridge	Distance
D244 (not observed)	-	-	-	-
D246	4.2 ± 0.1	Null	no	N/A
D253	< 2.8	Stabilizing	K311	2.6 Å
D271	< 2.8	Stabilizing	K268	2.7 Å
D292	< 2.8	Stabilizing	K279	4.0 Å
D302	< 2.8	Stabilizing	H305	3.0 Å
E307	3.9 ± 0.3	Stabilizing	R299	2.6 Å
D316	3.4 ± 0.1	Slightly Stabilizing	Maybe R325	5.1 Å
D317	< 2.8	Stabilizing	K237	2.7 Å
E323	3.6 ± 0.1	Stabilizing	unknown	unknown
D336	4.3 ± 0.3	Null	no	N/A

Five out of eleven signals from the ionizable residues in the I-domain show significantly changes in chemical shifts (see Table 1) whereas the other five remain unaffected upon pH change. For D246, E307, D316, E323 and D336 it was possible to obtain titration data and determine their corresponding pK_a values. For D246 the pK_a value was determined to be 4.2, differing only by 0.2 pH values from the pK_a of aspartate in a random coil, which is 4.0. The pK_a of D336 also is almost the same like in a random coil with 4.3. D316 had a pK_a value of 3.4, which is slightly lower than the pK_a of aspartate in a random coil and therefore it might contribute to the overall stability by participating in a salt bridge. The pKa value of E307 is 3.9,

0.5 pH units lower than the random coil pKa of 4.4 of glutamate. E323 differs with a pKa of 3.6 significantly from the random coil pKa. D253, D271, D292, D302 and D317 did not show any change in chemical shift upon pH change. The pKa for these residues consequently is lower than 2.8, the pH value where most proteins acid denature. The residues which show significantly lower pK_a values than in random coil are all are involved in salt-bridges in the structure of the I-domain (summarized in Table 1). One residue (D244) could not be assigned due to its location in the flexible D-loop, which causes NMR line broadening.

pH titration of His_6 tag and His305

The structure of the I-domain of bacteriophage P22 contains only one histidine at position 305 and an N-terminal His_6 metal affinity tag. The hydrogen atoms at the C-2 and the C-4 positions of the imidazole ring of histidine residues are easily resolved by 1D ^{1}H-NMR due to the unique downfield positions of their resonance signals. Changes in chemical shifts as a function of pH can thus be recorded and result in a titration curve, which allows the determination of the pK_a value (19). The protonated and deprotonated states of ionizable residues are almost always in rapid exchange on the NMR timescale (20), giving a population-averaged chemical shift of charged and neutral species. At high pH the deprotonated form dominates the chemical shift. As the pH is lowered, the resonance position gradually shifts toward the chemical shift of the protonated form, eventually reaching an acidic chemical shift plateau. The pH at the midpoint of the sigmoidal titration curve is the pK_a value (17). The pK_a value is typically determined from a nonlinear least-squares fit (Kaleidagraph, Synergy

Software) of the NMR chemical shifts versus pH to a modified Henderson-Hasselbalch equation (see Equation 1).

The contribution to the stability of a protein from having a histidine in a charged state at low pH compared to its neutral state at higher pH can be calculated from a thermodynamic linkage analysis (see Figure 9).

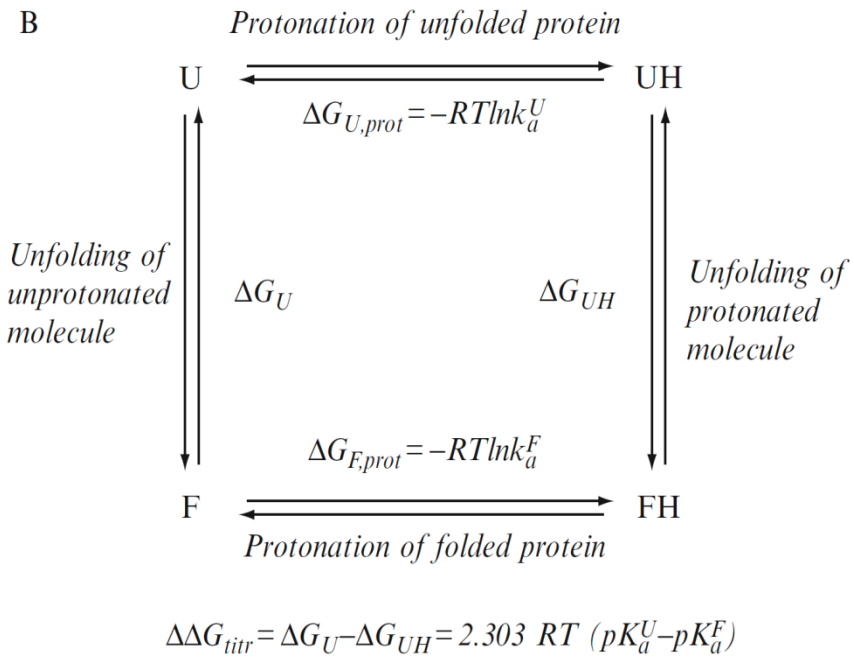

Figure 9: Thermodynamic linkage analysis

The thermodynamic linkage analysis is a means for quantifying the contribution of a change in charge to the change in stability. U is the unprotonated unfolded state, UH is the protonated unfolded state, F is the unprotonated folded state, FH is the protonated folded state and R is the gas constant (This scheme has been taken from Sheftic et al., 2009 (17))

H305 is in a salt bridge with D302

The pK_a value of a histidine in an unstructured random coil conformation at 25°C is 6.5. This value was obtained from the peptide Gly-Gly-His-Gly-Gly and is a baseline value for what the ionization should simply be from chemistry, in the absence of any structure (21). Compared to the pK_a value of that histidine in an unstructured random coil conformation, the pK_a value for the His_6-tag in the I-domain is 6.68 ± 0.05, which is almost the same pK_a value as for histidine in a random coil conformation. This shows that the His_6-tag lacks any secondary structure and is not involved in any electrostatic interactions in the protein. According to the non-linear least square fit, the pK_a for His305 is 9.05 ± 0.04, which is 2.55 pH units higher than the one in a random coil conformation (Figure 10). According to the thermodynamic cycle calculation (Figure 9) the charged state of His305 favors the folded state of the I-domain by 3.48 kcal/mol compared to the neutral state of His305 at high pH values.

Since the pK_a of His305 is significantly higher than that of a histidine in a random coil conformation, it can be expected that H305 has a much higher affinity for protons. This higher affinity for protons could be satisfied by the interaction with negatively charged (acidic) residues like glutamate and aspartate, for example by formation of a salt bridge. The structure of the I-domain suggests that His305 might interact with an aspartic acid at position 302 (D302) (see Figure 11). D302 is located in the β4-β5 turn of the structure and lies within 3.0 Å distance to His305.

Site directed mutagenesis was introduced to look at the stability contribution to the I-domain by the ionic interaction between H305 and D302. Two single mutants of the WT I-

domain were constructed by replacing each the histidine and the aspartate with alanine. The first step in a series of experiments was to determine the thermodynamic stability of the mutations upon pH change.

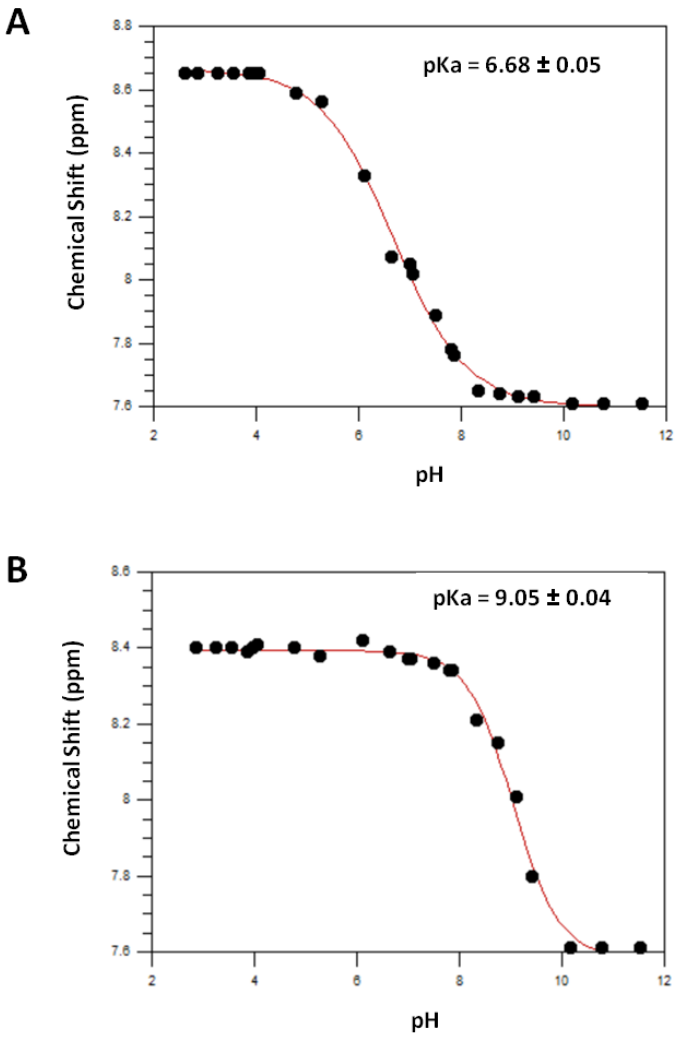

Figure 10: pH titration of His_6-tag and H305 from WT I-domain from bacteriophage P22

(A) shows the pH-titration of the His_6-tag of the I-domain and the corresponding pK_a value. (B) depicts the pH-titration of H305 with the corresponding pK_a value. The chemical shifts were obtained from 1D-1H-NMR experiments as a function of pH. The fit of the data is marked by the solid red line.

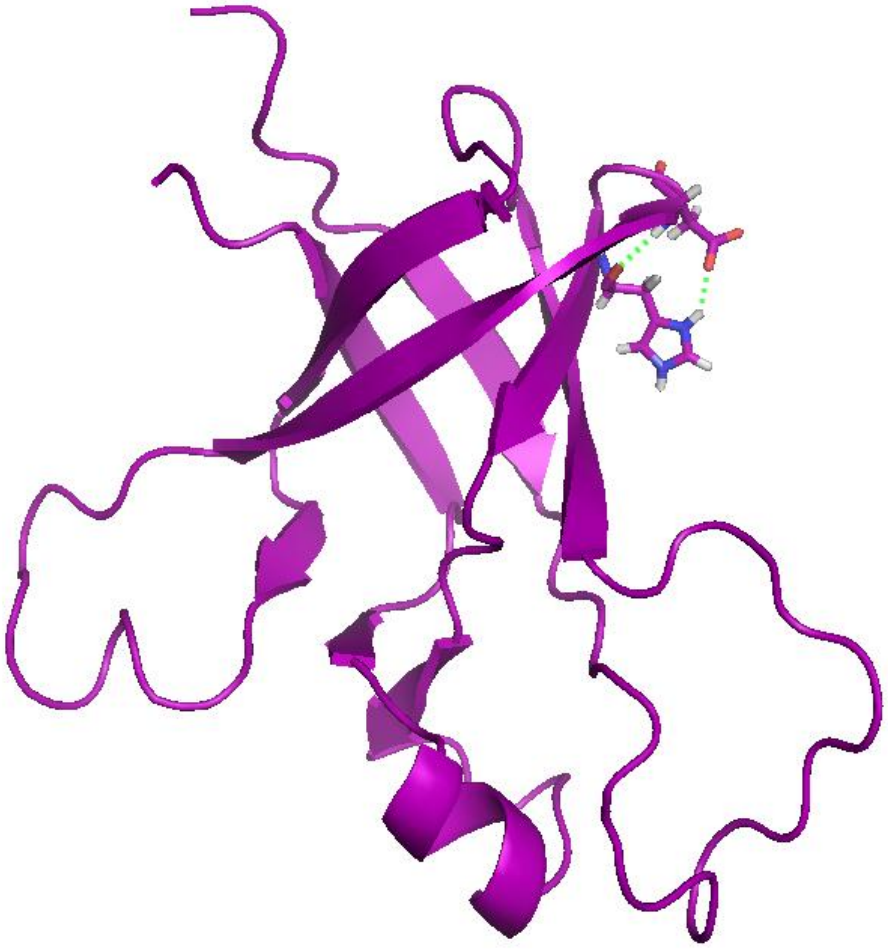

Figure 11 High resolution NMR structure of the P22 I-domain

NMR structure (cartoon) of the I-domain shown in magenta. Residues H305 and D302 are highlighted in atom colors and shown as stick presentation. Both residues are connected via two hydrogen bonds, one between the backbone and the second between the side chains, indicated by the green dotted lines.

Chapter 3

Urea Denaturation Experiments

Urea Equilibrium Denaturation Experiments of D302A and H305A I-domain

Circular dichroism spectroscopy (CD) experiments were done to determine the thermodynamic stability of the H305A and D302A I-domain as a function of pH. In these experiments, H305A and D302A I-domain at a concentration of 14 µM were incubated in 0-6 M urea in 20 mM phosphate buffer at 20°C until equilibrium was established. The CD signal at 220 nm was used to examine the unfolding transition at different pH values. The data were fit to a standard two-state thermodynamic model to determine the standard free energy of unfolding (ΔG_0) as function of pH.

Many proteins have been found to closely approach a two-state mechanism

$$N \rightleftharpoons D$$

Equation 2

Where only the native state, N, and the denatured state, D, can be found primarily in the transition regions. The ellipticity is measured as a function of the denaturant concentration and is characteristic of the native state, y_N, and the denatured state, y_D. These are determined in the transition region through extrapolating the high and low plateau regions of the denaturation curve. In a two-state mechanism,

$$f_N + f_D = 1$$

Equation 3

and

$$y = y_N f_N + y_D f_D$$

Equation 4

where f_N and f_D correspond to the fraction of the protein present in the native and denatured states, respectively (22).

Equilibrium constants in the transition region are determined through extension of the pre- and post-unfolding base lines into the transition region. Mathematically these extensions are represented by equation

$$\Delta\epsilon_N = \Delta\epsilon^0{}_N + m_N[D]$$

Equation 5

$$\Delta\epsilon_U = \Delta\epsilon^0{}_U + m_U[D]$$

Equation 6

where $\Delta\epsilon^0{}_N$ and $\Delta\epsilon^0{}_U$ correspond to the different CD signals for native and unfolded protein as function of denaturant concentration, $[D]$, and are determined at given denaturant concentrations in the transition region. $\Delta\epsilon^0{}_N$ and $\Delta\epsilon^0{}_U$ are intercepts, and m_N and m_U are slopes of the pre- and postfolding plateaus, respectively. Combining these equations,

$$K_{obsd} = {\left(\Delta\epsilon^{0}{}_{N} - \Delta\epsilon\right)}/{\left(\Delta\epsilon - \Delta\epsilon^{0}{}_{U}\right)}$$

Equation 7

these baselines are used as reference points in the transition zone and help determine equilibrium constants for unfolding at given concentrations of denaturant and corresponding $\Delta\epsilon$ values. K_{obsd} corresponds to the equilibrium ratio of unfolded/native protein species at any given denaturant concentration. The observed equilibrium constants determined in the transition region are converted to free energy values (ΔG_{obsd}).

$$\Delta G_{obsd} = \Delta G^{0}{}_{N-U} + m[D]$$

Equation 8

$\Delta G^{0}{}_{N-U}$, the intercept is the free energy change for unfolding in the absence of denaturant, m is the slope and $\Delta G_{obsd} = -RT \ln K_{obsd}$.

Equation 5 to Equation 8 can be combined into a single equation relating $\Delta\epsilon$ and denaturant concentration, $[D]$, with $\Delta\epsilon^{0}{}_{N}$, $\Delta\epsilon^{0}{}_{U}$, m_N, m_U, m_G and $\Delta G^{0}{}_{N-U}$ as fitting parameters (23).

$$\Delta\epsilon = \frac{\left[\left(\Delta_{\epsilon_N} + m_N[D]\right) + \left(\Delta_{\epsilon_U} + m_U[D]\right) * exp - (\Delta G^{0}{}_{N-U}/RT + m[D]/RT)\right]}{[1 + exp - (\Delta G^{0}{}_{N-U}/RT + m[D]/RT)]}$$

Equation 9

D302A shows a significantly lower thermodynamic stability than H305A

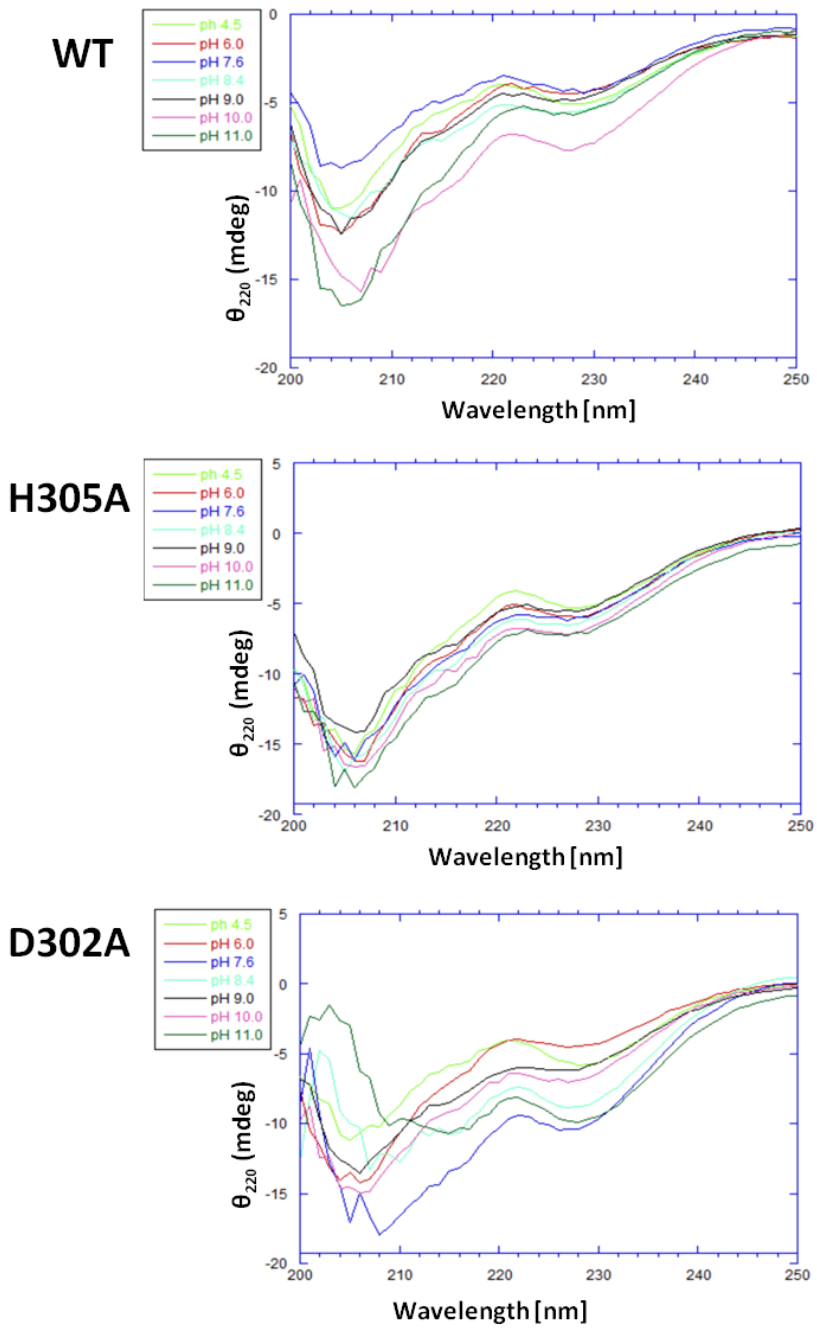

Figure 12: Wavelength scans at differerent pH values for WT, H305A and D302A I-domain

CD signal of WT, H305A and D302A I-domain at a concentration of 14 µM at different pH values in the absence of urea was measured over a wavelength range from 250 to 200 nm to determine proper folding. Since D302A was already unfolded at pH 11, equilibrium urea denaturation experiments were not performed at this pH.

The stability of the H305A and D302A I-domain as a function of pH were determined using circular dichroism (CD) experiments. The stability of the WT I-domain decreased by about 3 kcal/mol at basic pH values. The WT I-domain is most stable between pH 6.0 and 7.6 (experiments done by LaTasha Fraser, 2013). This behavior is predicted by the pK_a of His305 in WT I-domain (see Figure 10).

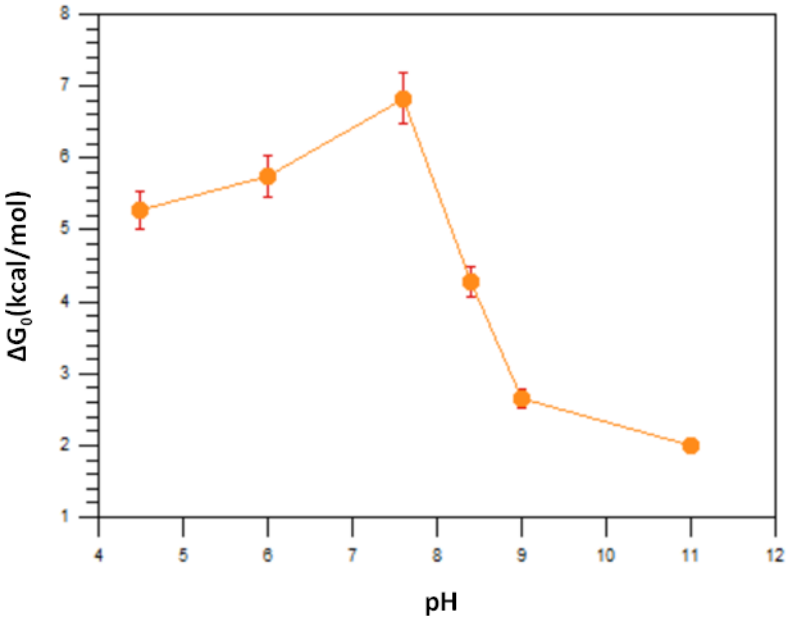

Figure 13: WT I-domain ΔG_0 values obtained from CD experiments as a function of pH

An overall decrease in stability of about 4 kcal/mol was expected for H305A and D302A since the stabilizing electrostatic interaction of the salt bridge is disrupted by these substitutions. However, the free energy change for H305A was about the same as for WT I-domain. At pH 6.0, WT I-domain has a ΔG_0 of 5.8 ± 0.3 kcal/mol and the ΔG_0 for H305A was determined to be 6.3 ± 0.2 kcal/mol. The results for the equilibrium unfolding urea titration of D302A did match the expectations, showing a significantly decreased ΔG_0 of 3.3 ± 0.2 kcal/mol

at pH 6.0 compared to WT I-domain. It was also predicted that additionally to the decreased stability the ΔG_0 for these mutants would be invariant with pH. Both mutants, H305A and D302A, are invariant upon pH change due to disruption of the salt bridge (see Figure 14).

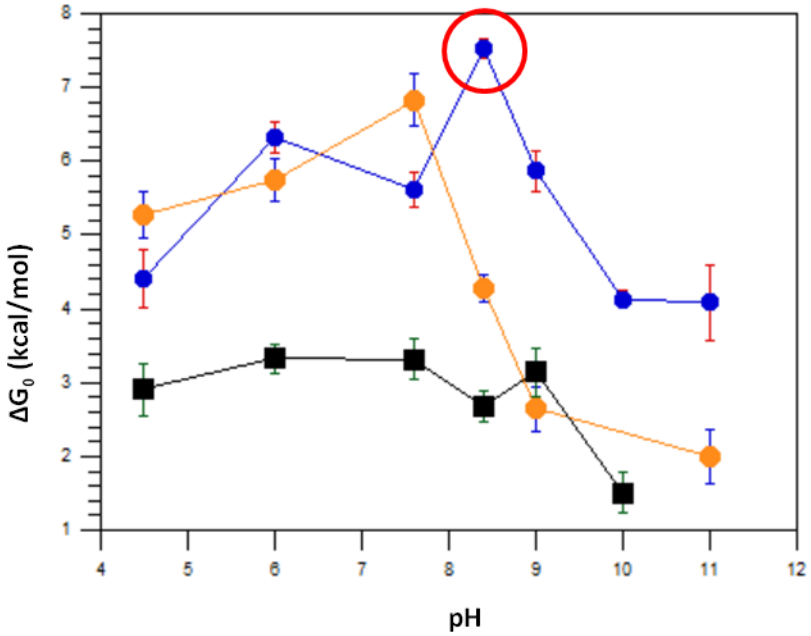

Figure 14: Overlay of WT, H305A and D302A I-domain ΔG_o values obtained from Circular Dichroism experiments as a function of pH dependence

WT (orange data), H305A (blue data) and D302A (black data) I-domain ΔG_0 values obtained from circular dichroism equilibrium unfolding urea titration experiments (at 220 nm) as a function of pH. The data point of ΔG_0 of H305A at pH 8.4 (in red circle) can be regarded as an outlier.

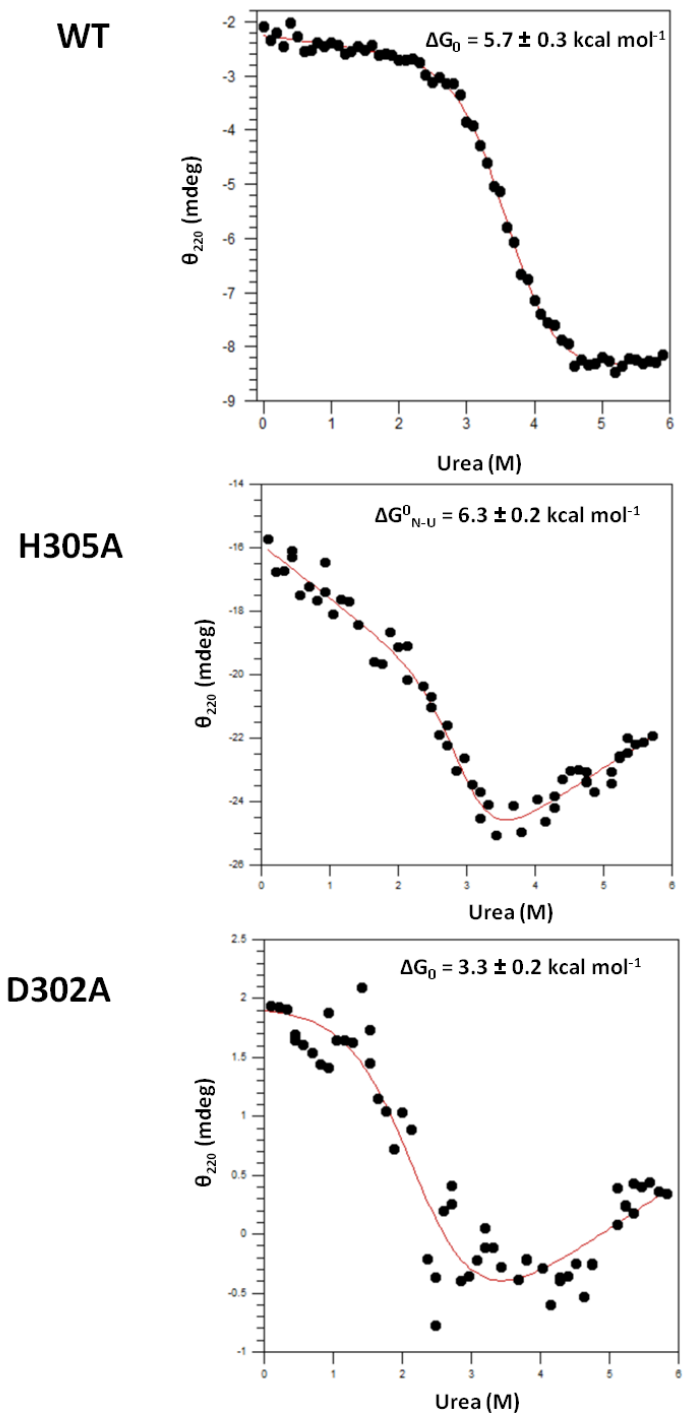

Figure 15: Representative equilibrium unfolding urea titration at pH 6.0

WT, H305A and D302A I-domain were titrated to give final urea concentrations between 0 and 6 M in 20 mM phosphate buffer at pH 6.0 and incubated at 20°C. The final concentration of I-domain was 14 µM. The solid red line is the fit of the data. WT I-domain experiments were done by LaTasha Fraser.

Determination of melting transition of H305A and D302A I-domain via Circular Dichroism

For H305A and D302A I-domains a thermally induced decrease in CD signal can be observed, which can be used to monitor the melting transition. These were compared to the melting transition of WT I-domain. Samples of WT, H305A, and D302A I-domain (14 µM in 20 mM phosphate buffer, pH 7.6) were ramped from 20 to 75°C (65°C for D302A I-domain). At each 0.5°C increment in temperature the CD signal at 220 nm was recorded. The melting temperature (T_m) was determined from a nonlinear least squares fit of the ellipticity as a function of temperature according to the following equation (24)

$$f(T) = \frac{\alpha_N + \beta_N T + (\alpha_D + \beta_D T)e^{-[\Delta G^\circ_{D-N}(T)]/RT}}{1 + e^{-[\Delta G^\circ_{D-N}(T)]/RT}}$$

Equation 10

where f is the ellipticity at a given temperature (T). The parameters α_N, β_N, α_D and β_D define the ellipticity at the native (N) and the denatured states (D). α and β describe a line with a slope equal to β and a y-intercept equal to α. The transition midpoint of the curve defines T_m (24).

D302A has a significantly lower melting temperature than H305A

According to the nonlinear least square fits of the ellipticity versus temperature plots of WT, H305A and D302A I-domain the T_m of WT I-domain was 50.2 ± 0.03 °C. H305A I-domain T_m was determined to be 48.5 ± 0.54 °C and the one of D302A 33.8 ± 0.10 °C, which is significantly lower than WT. These results confirm the outcome of the equilibrium urea denaturation

experiments demonstrating a highly decreased stability for D302A while H305A shows almost the same stability like WT I-domain.

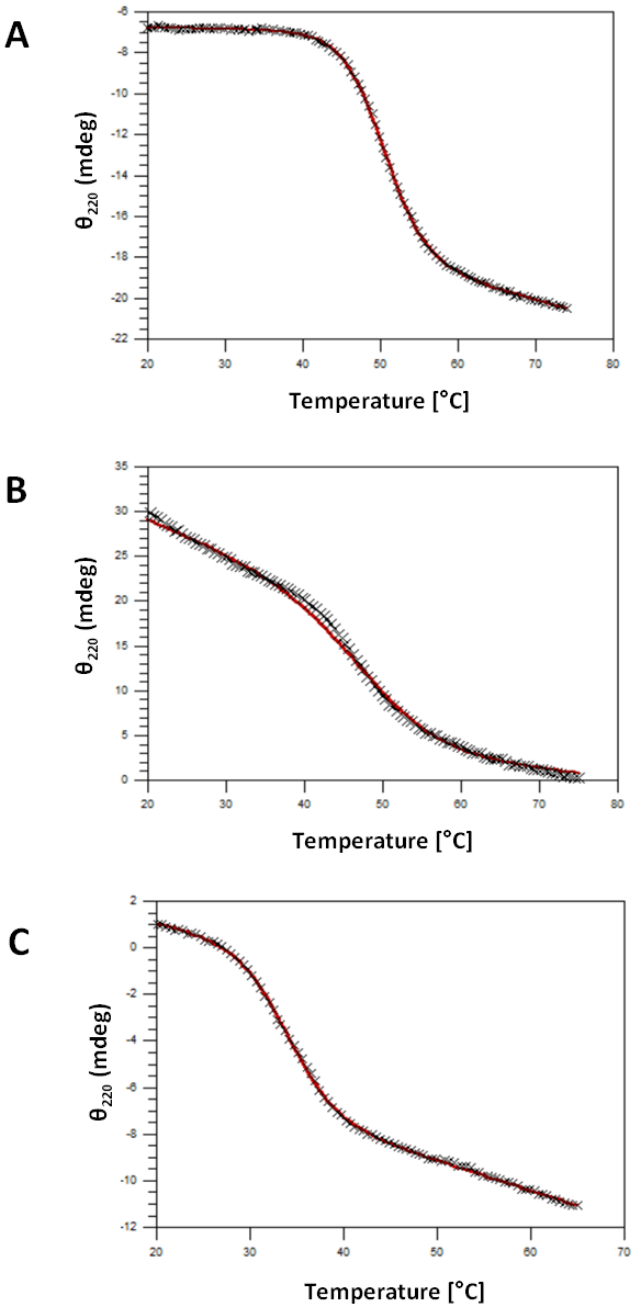

Figure 16: Comparison of melting transition of WT, H305A and D302A I-domain

The melting temperature of WT, H305A and D302A I-domain was determined by increasing the temperature from 20 to 75°C (65°C in the case of D302A) and measuring the CD signal at 220 nm at every 0.5 °C. The melting temperature was determined from a nonlinear least square fit.

Chapter 4

Hydrogen-Deuterium-Exchange Experiments

Hydrogen Exchange experiments of H305A and D302A via NMR

Hydrogen-Deuterium exchange (HX) experiments were performed with H305A and D302A I-domain to show which amide protons are protected from solvent exchange. WT I-domain HX experiments were already done by LaTasha Fraser. In a protein, amide protons are in a constant exchange with solvent protons. For the amide protons that are exposed on the surface of a protein and therefore solvent-accessible, this exchange is happening at a faster rate than for the ones which are buried in the core of the protein and involved in hydrogen bonds in secondary structure elements. For these solvent-inaccessible amide protons the exchange is occurring at a significantly slower rate (see Figure 17). Exchange rates are also dependent on the temperature and the pH. In a ^{1}H-^{15}N correlation experiment, like a 2D ^{1}H-^{15}N-HSQC experiment, these amide proton exchanges can be measured. (25). The protein sample is first lyophilized and then dissolved in D_2O and solvent-accessible amide protons are exchanged eventually. Once these amide protons exchanged with the solvent they no longer show a correlating peak in the HSQC spectrum. The HX experiments were performed at a pH of 6.0.

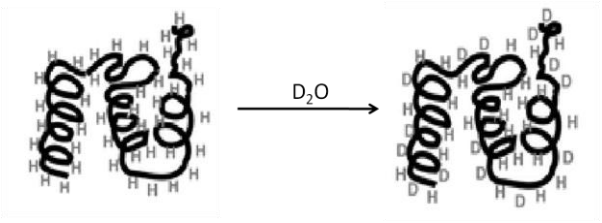

Figure 17: Schematic illustration of hydrogen-deuterium exchange

This figure illustrates how solvent exposed protons exchange with deuterium in the solvent while protons in the protein core are protected from exchange (modified from Hoofnagle et al., (26))

The degree of protection for each residue can be expressed as a site-specific equilibrium constant for the "opening" reactions which result in exchange-competent conformations provided that the protein is undergoing exchange within EX2 conditions (27; 28) (shown by LaTasha Fraser, data not published).

Equation 11

$$K_{op} = \frac{k_{obs}}{k_{int}}$$

where k_{obs} is the experimental exchange rate and k_{int} is the intrinsinic exchange rate, normally determined by exchange rates in short, unstructured peptides (29) determined via the program Spheres (30). The change in Gibbs free energy for opening reactions that promote exchange is:

Equation 12

$$\Delta G_{HX} = -RTln(K_{op})$$

where R is the gas constant and T the absolute temperature (28).

H305A and D302A are likely to cause perturbations in the I-domain structure

Before the HX experiments, H305A and D302A ^{1}H-^{15}N-HSQC experiments were performed in water to check for protein folding and solubility and subsequently the spectra were compared to WT I-domain in H_2O. For some of the residues in H305A and D302A large chemical shift changes were observed when compared to WT I-domain (see Figure 19). Structural mappings reveal that most of these shifting residues are clustered in the same or

directly adjacent β-sheets of the mutated residues. Only very few are located in the α-helix, loop or terminal regions (see Figure 20). This indicates a perturbed structure induced by the mutations.

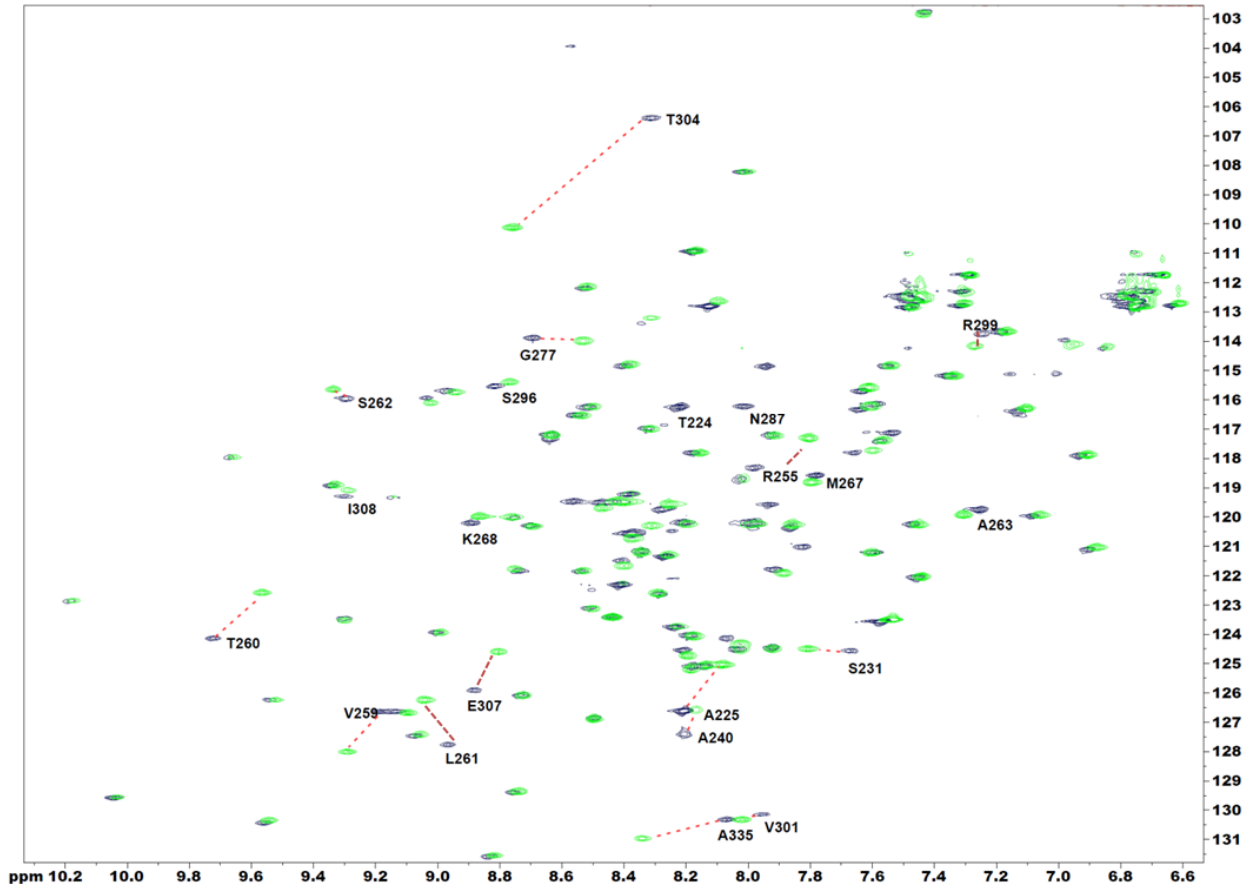

Figure 18: Overlay of WT I-domain spectrum (blue) and H305A (green)

Overlay of 2D ^{1}H-^{15}N-HSQC spectrum of WT I-domain shown in blue and H305A spectrum shown in green. The NMR experiments were performed at pH 6.0 and at 25°C.

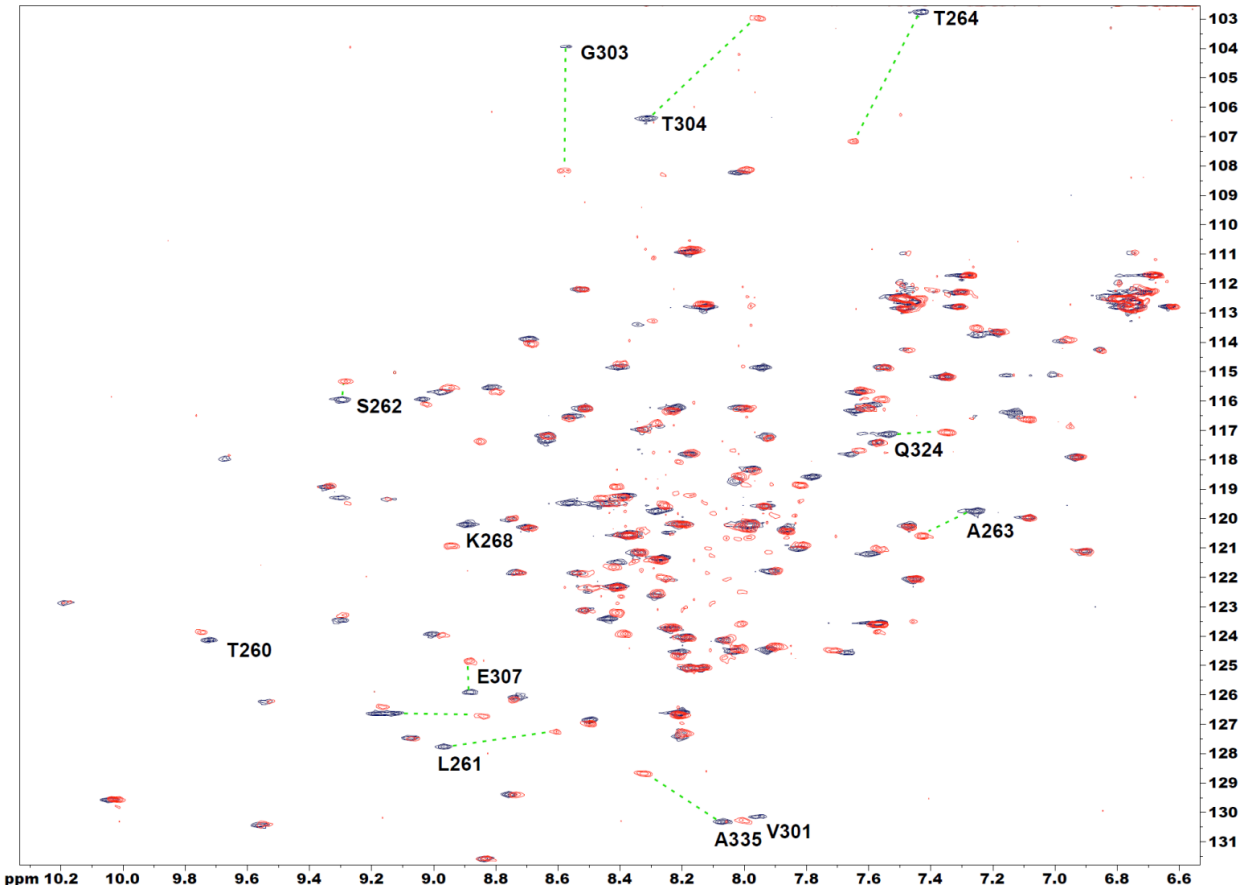

Figure 19: Overlay of WT I-domain spectrum (blue) and D302A (red)

Overlay of 2D ^{1}H-^{15}N-HSQC spectrum of WT I-domain shown in blue and D302A spectrum shown in red. The NMR experiments were performed at pH 6.0 and at 25°C.

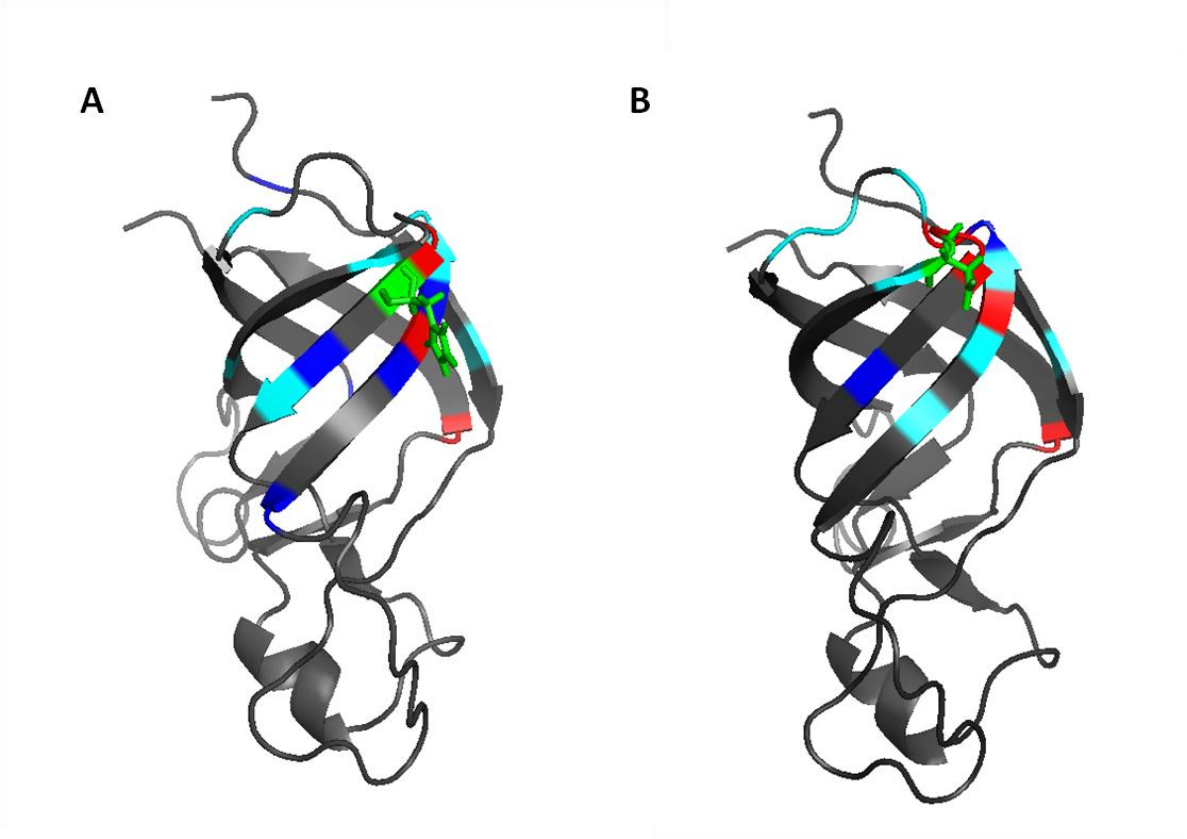

Figure 20: Structural mapping of shifting residues in WT and H305A and D302A spectra

Panel A shows the mapping of shifting residues in WT and H305A spectra, Panel B the shifting residues compared from WT to D302A. Residues H305A and D302A are highlighted in green and shown in stick presentation. Residues which showed strong shifts (> 2 ppm) are colored in red, medium shifting ones (1-2 ppm) are colored in blue and weak shifts (0.5-1 ppm) are shown in cyan. The same scale was used for H305A and D302A.

D302A exchanges at faster rates than H305A in HX experiments

For H305A it was possible to detect 42 residues (34%) from the original 123 residues in the I-domain after about 60 minutes in D_2O at pH 6 and 25°C. By contrast, only about 18 residues (14%) from D302A have amide protons that persist longer than 70 minutes in D_2O (see Figure 21). In WT I-domain 54 residues (44%) were detected after an average of 40 minutes in D_2O. These residues are involved in secondary structure elements and therefore are protected

from solvent exchange. The residues that are not involved in secondary structure elements exchange too fast to be detected and are no longer visible as peaks in the ^{1}H-^{15}N-HSQC spectrum. The residues that were protected from solvent are all involved in secondary structure elements and are shown to have the highest ΔG_0 values. The most protected residues are located in the β-sheets, mainly in the six-stranded β-barrel. The highest $\Delta G_{0,\ HX}$ values were obtained for β-strands 4 and 5 which shows a highly cooperative stabilization for this region. β-strand 1 is completely missing in the ^{1}H-^{15}N-HSQC spectrum of D302A indicating a weaker protection. The α-helix which is comprised of residues 322-326 seems to be almost completely unprotected with only one residue (A328) to be detected for H305A. A328 is found on the outer tip of the helix close to β-strand 6. The $\Delta G_{0,\ HX}$ value obtained for about 20% of the most protected residues in H305A HX experiments is 6.2 ± 0.4 kcal/mol which compares to 6.3 ± 0.2 kcal/mol determined from equilibrium unfolding transitions monitored by CD, which is represented by the green horizontal line in Figure 23. The $\Delta G_{0,\ HX}$ value for D302A was determined to 4.3 ± 0.3 kcal/mol, which is about 1 kcal/mol larger than the 3.3 ± 0.2 kcal/mol obtained from the CD experiments (see Figure 23). For WT I-domain the average $\Delta G_{0,\ HX}$ value of 8.3 kcal/mol is about 2.1 kcal/mol bigger than the ΔG_0 determined by CD. Although there are some discrepancies between ΔG_0 values obtained from CD and HX, these differences have been observed for other proteins before (27), (28). In the example of RNase A the $\Delta G_{0,\ HX}$ value is 4.2 kcal/mol, 1.6 kcal/mol higher than the ΔG_0 value determined by fluorescence (27). One explanation for this phenomenon is that residual structures in the denatured state could protect amide protons from exchange and thus lead to increased $\Delta G_{0,\ HX}$ values (27). Another reason is an increased protein stability of 0.3 kcal/mol which has been reported when dissolving

proteins in D_2O instead of H_2O (28), (27). Furthermore, the isomerization state of the prolines in the protein structure can lead to discrepancies between thermodynamic free energy changes determined by CD and HX. The I-domain of P22 contains four prolines, whereas one of them is in *cis* conformation. According to the proline-dependent free energy increment (27), the proline isomerization is calculated to contribute 0.94 kcal/mol to ΔG_0 determined by CD at 20°C. Together with D_2O contributions this would lead to a corrected ΔG_0 of 7.5 kcal/mol for H305A and 4.5 kcal/mol for D302A.

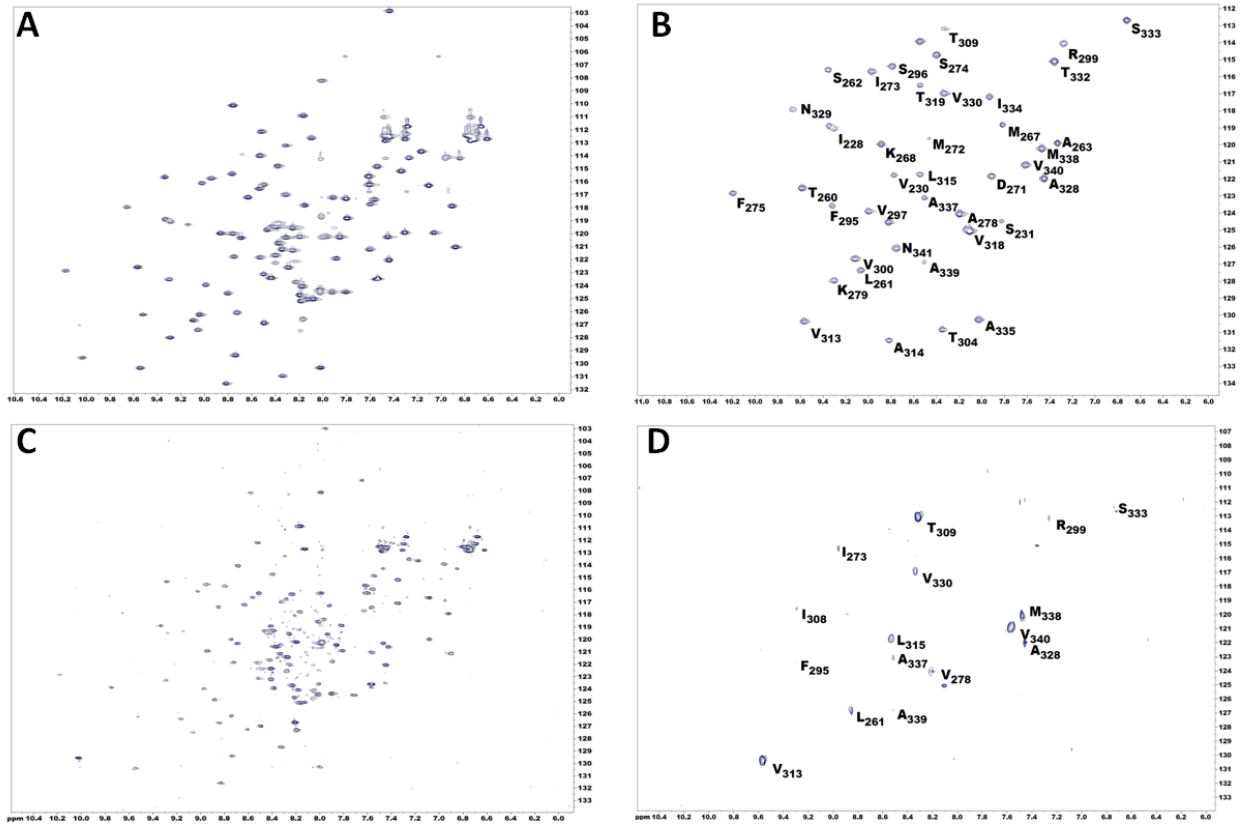

Figure 21: Representative spectra of Hydrogen Exchange in H305A and D302A I-domain

Panel A shows the ^{1}H-^{15}N HSQC spectrum of H305A in water, panel B the exchange of H305A after 52 minutes in D_2O at pH 6 and 25°C. Panel C shows the ^{1}H-^{15}N HSQC spectrum of D302A in water, panel D the exchange of D302A after 70 minutes in D_2O.

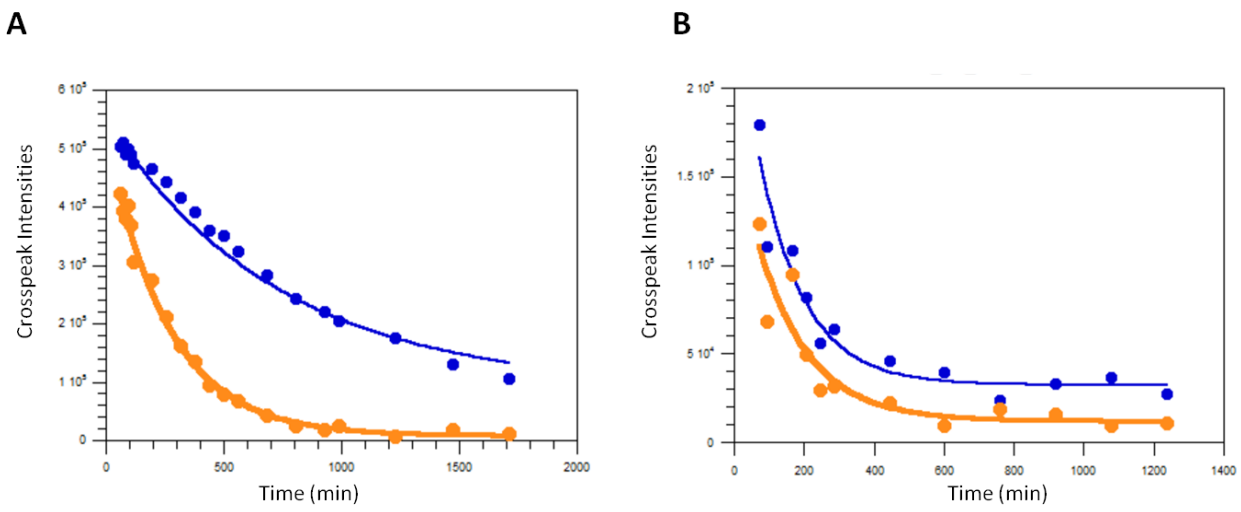

Figure 22: Representative data for exponential decay of ^{1}H-^{15}N crosspeak intensities

Panel A shows the exponential decay of ^{1}H-^{15}N crosspeak intensities of the representative residues L261 (shown in blue) and L314 (shown in orange) in H305A, for D302A in Panel B. The apparent exchange rate was determined from the nonlinear fit of the exponential decay (solid lines).

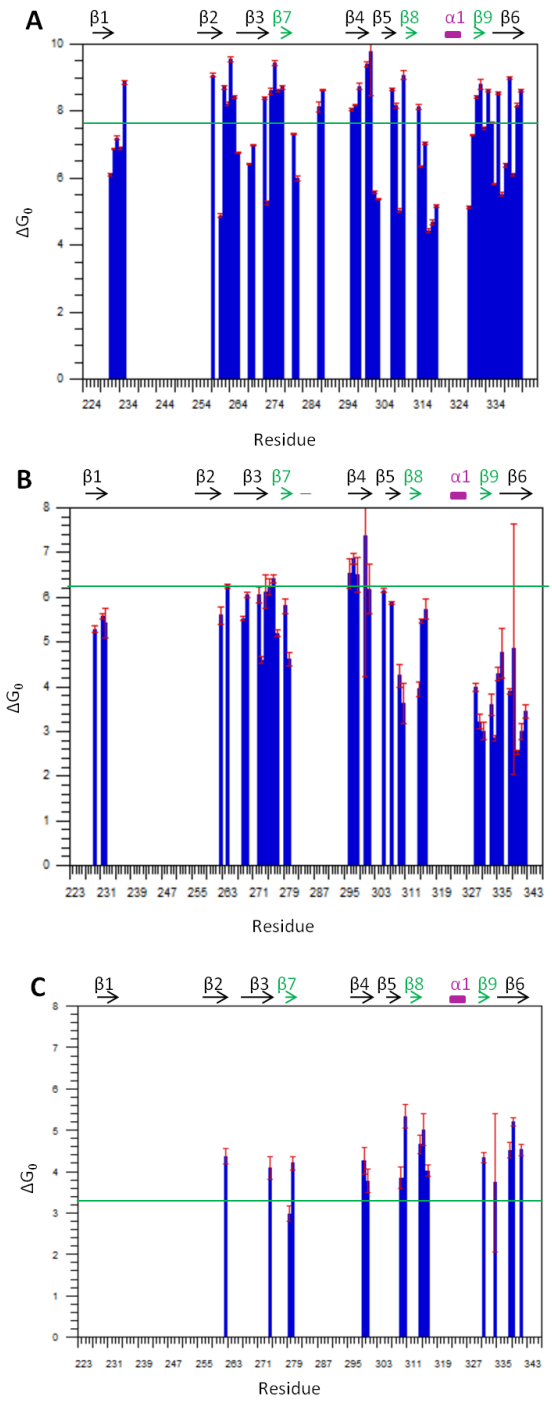

Figure 23: Sequence dependence of thermodynamic free energy change from HX experiments

Panel A represents the thermodynamic free energy change of WT I-domain, panel B the thermodynamic free energy change of H305A and panel C D302A. Blue columns show the thermodynamic free energy change due to unfolding $\Delta G_{0,\,HX}$, whereas the green horizontal lines depicts ΔG_0 determined at pH 6.8 from the unfolding transitions determined by CD.

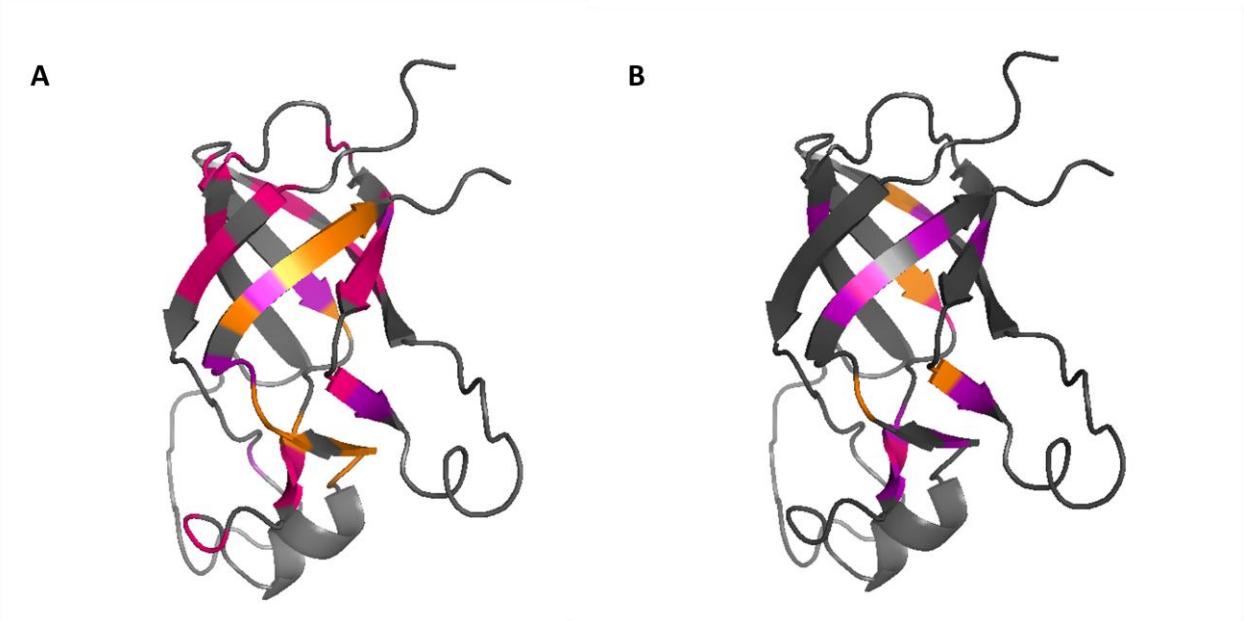

Figure 24: Structural mapping of $\Delta G_{0,\,HX}$ values

Panel A shows the structural mapping of ΔG_0 values obtained from NMR HX experiments of H305A, Panel B of D302A. The most stable regions (ΔG_0 higher than 5 kcal/mol) are colored in pink and regions with average ΔG_0 values (between 4 and 5 kcal/mol) are shown in purple. The least stable regions with ΔG_0 values less than 4 kcal/mol are colored in orange. Grey regions in the structure represent the residues which exchanged too fast to be detected. The same scale was used for H305A and D302A.

Chapter 5

Conclusions, Discussion & Future Work

The nonconserved accessory domain of bacteriophage P22 was shown to have an important role in the assembly and stability of coat proteins. The high resolution structure of the I-domain solved by Rizzo et al. (12) shows that it adopts an antiparallel six-stranded β-barrel fold with a β-sandwich containing three smaller β-strands and an additional small, 1.5 turn helix.

In this study the electrostatic interactions within the I-domain were investigated. pH titration experiments with NMR have shown that 7 out of 11 acidic residues within the I-domain are most likely involved in electrostatic interactions according to their apparent pK_a values. These residues are D253, D271, D292, D302, D317, E307 and E323. The main focus in the following experiments was on the hydrogen-bonded salt bridge between H305 and D302. This salt bridge stabilizes a tight turn between sheets β4 and β5 in the structure. Site-directed mutagenesis experiments with H305A and D302A substitutions were performed to investigate the affects of these single mutations on I-domain stability. The thermodynamic stability of H305A and D302A was determined with urea equilibrium denaturation experiments monitored by CD. The ΔG_0 value for D302A at pH 6.8 was determined to 3.3 ± 0.2 kcal/mol and thus is significantly lower than 6.2 ± 0.3 kcal/mol for WT I-domain at pH 6.8. H305A showed almost the same stability like WT with a ΔG_0 value of 6.0 ± 0.2 kcal/mol. Temperature melt experiments confirmed a weaker stability for D302A compared to H305A with a significantly lower melting temperature of 33.8°C compared to 48.5°C for H305A and 50.2°C for WT.

In NMR HX experiments, the highest $\Delta G_{0,\ HX}$ values were observed for the β-sheets, primarily those found in the β-barrel core of the protein. The $\Delta G_{0,\ HX}$ values for about 20 % of the most protected residues from HX experiments were 6.2 ± 0.4 kcal/mol and 4.3 ± 0.3 kcal/mol for H305A and D302A, respectively. Both values are significantly lower than the determined $\Delta G_{0,\ HX}$ of 8.3 kcal/mol for WT by HX. Important to notice in this context are the notably lower $\Delta G_{0,\ HX}$ values for strand β_1 and β_6 in H305A. These strands seem to have a lower stability than strands β_2 to β_5. In the HX data for D302A after 70 minutes β_1 residues are completely missing and most of the amides in sheets β_1 to β_3 have disappeared. A weak protection for the residues in the first β-strand has already been observed for WT I-domain, most likely because these residues are only interacting with a single β-strand instead of being sandwiched between two neighboring β-sheets. Additionally, β_1 shows misalignment with strand β_2 caused by a kink at residues S231 and G232. Generally, the residues of D302A show a weaker protection in comparison to H305A, shown by the faster exchange. Of 123 residues, only 18 were detected in D302A after 70 minutes. These residues are strongly protected and also experience the slowest exchange in H305A and WT.

Efficient folding of coat protein in viruses is crucial for virus maturation. The I-domain of bacteriophage P22 increases stability of monomeric coat proteins and thus no chaperones are required for proper folding, unlike some other HK97-like viruses (15). Electrostatic interactions within the I-domain of bacteriophage P22 contribute to the stability of the I-domain itself and consequently also for coat protein. The focus of this study were residues D302 and H305 that were substituted with alanines to investigate their contribution to I-domain stability. The outcomes were that D302A is significantly less stable than H305A in the isolated I-domain of

bacteriophage P22. H305A and D302A mutations were also introduced into full-length coat protein of P22 to investigate affects on capsid assembly and stability. In phage, full-length coat protein H305A causes no phenotype and phage are produced. By contrast, D302A causes a temperature-sensitive phenotype (data not published) and D302G is a *tsf* substitution (14). These results fortify the results from experiments done with isolated I-domain showing that D302A greatly affects the structure and stability of the I-domain and thus affects capsid assembly and stability, whereas H305A has no major impacts. The reasons why the substitution of H305 to alanine did not show any significant affects on I-domain stability, remain unclear so far and need to be further investigated. Other electrostatic interactions within the I-domain that might contribute to its overall stability (involving residues D253, D271, D292, D316, E307, D317 and E323) may be topic of future studies. Mutation studies of these residues can elucidate whether these residues are necessary to maintain I-domain stability.

Chapter 6

Materials and Methods

H305A and D302A I-domain expression and purification

The gene encoding for the I-domain of bacteriophage P22, comprising amino acids S223-V345 of the full-length coat protein was previously cloned into *pET30b* plasmid and expressed in *E.coli* BL21 (DE3) cells (done by M. Suhanovsky). Standard site-directed mutagenesis was used to construct two single mutants of the wild-type protein to eliminate the salt bridge between His305 and Asp302. Both residues were replaced by alanine. Point mutation H305A was generated previously and D302A I-domain was generated following a site-directed mutagenesis protocol. The mutated plasmid was sequenced by Genewiz (South Plainfield, NJ) to verify the mutation in the plasmid. Kanamycin resistant cells were plated, selected and grown in LB-media to mid-log phase with 40 µg/mL of kanamycin at 37°C. Isotopic labeling was accomplished by using 1 g/L $^{15}NH_4Cl$ in M9 minimal media for cell growth. Expression was induced with 1 mM isopropyl β-D-1-thiogalactopyranoside (IPTG) and allowed to continue for 16 hours at 30°C. For D302A I-domain expression was allowed to continue for about 16 hours at 16 °C due to weak expression at 30 °C. Cells were cooled on ice and harvested via sedimentation for 15 minutes at 35000 x g in an SLC 6000 rotor (Sorvall). The cells were resuspended in 20 mM phosphate buffer (pH 7.6) containing a 1:100 dilution of EDTA-free protease inhibitor cocktail P8849 (Sigma, St. Louis, MO), 0.1% w/v Triton X-100, lysozyme (200 µg/mL), 5 mM $MgSO_4$, 0.5 mM $CaCl_2$ and 100 µg/mL DNase and RNase. Cells were lysed by one freeze/thaw cycle and following sonication with a regular probe on the sonicator (Misonix). The amplitude was set to 35 seconds, the pulsing time was set to 15 seconds on-time and 30

seconds off-time with the on-time adding up to 2 minutes. Cell debris was removed by centrifugation in a Sorvall F18-12 x 50 rotor at 32000 x g for 15 minutes. To remove any membranes the supernatant underwent ultracentrifugation in a T-865 rotor at 162000 x g for 40 minutes. The supernatant was loaded onto a 15 mL Talon metal-affinity column (Clontech, Mountain View, CA) for purification. The column was washed with 60 mL of buffer containing 10 mM imidazole and elution was carried out with 60 mL buffer containing 250 mM imidazole. Fractions containing I-domain were determined by SDS-PAGE, pooled, dialysed three times (3 x 2L) against 20 mM sodium phosphate buffer (pH 7.6) and concentrated in a Centricon with a 10K nominal molecular weight cut-off filter from Millipore (Billerica, MA).

NMR spectroscopy

pH titration of I-domain and Histidines

NMR experiments were performed with two samples of 600 µL containing 0.33 mM I-domain in D_2O. One sample was used to perform the acid titration experiments, the other sample was used for the base titration. pH values were adjusted using 1 M HCl and 1 M NaOH. ^1H chemical shifts were referenced to internal DSS. Experiments were collected on a Varian Inova 600 MHz spectrometer at a temperature of 37°C. 1D 1H-NMR experiments were collected at different pH values and data were processed using Felix-NMR (San Diego, CA).

pH titration of acidic residues in the I-domain

The ^{15}N-labeled I-domain samples for the titration experiments were dissolved in H_2O/D_2O (90%/10%) and 1 µL DSS was added as internal standard. The final concentration of I-domain in the sample was 1.62 µM. The pH was adjusted using diluted HCl and NaOH and determined using a pH meter (Mettler Toledo MA 235) equipped with a glass electrode (Mettler Toledo InLab Micro, pH 0-14) before and after data acquisition. The two values agreed within 0.1 pH unit and were averaged for the data fitting. The pH values ranged from 2.33 to 11.18. The NMR experiments were performed on a Varian Inova 600 MHz spectrometer equipped with a cryogenic probe at a temperature of 37°C. The titration data were obtained from a series of 2D Nuclear Overhauser Effect Spectroscopy (NOESY) and HSQC.

Hydrogen-Deuterium Exchange Experiments

NMR HX experiments were performed on 0.1 mM ^{15}N-labeled D302A and 0.5 mM ^{15}N-labeled H305A I-domain sample in 20 mM sodium phosphate buffer, pH 7.6 which were lyophilized and then dissolved in D_2O and brought to pH 6.0 with DCl right before data collection. A 300 µL sample volume contained in Shigemi microcells was used for NMR experiments. Data were collected on a 600 MHz Varian INOVA spectrometer equipped with a cryogenic probe at a temperature of 25 °C. Data were processed using iNMR (Nucleomatica, Molfetta, Italy) and Felix (Felix NMR, San Diego, CA). The free energy change was calculated using Equation 12. Uncertainties for the free energy change were calculated using standard error propagation (28). The obtained ^{1}H-^{15}N crosspeak intensity was plotted as a function of time and fitted against an exponential decay to determine the experimental rate. Intrinsic rates were calculated with the program Sphere (30).

Circular Dichroism

Urea Denaturation

H305A and D302A I-domain solutions were diluted to a final concentration of 0.4 mg/mL and mixed using a Hamilton Microlab 50 titrator to final urea concentrations ranging from 0 M to 6 M in 0.1 M increments (22). Final urea concentrations were measured with a refractometer (Carl Zeiss, Germany). Samples were incubated overnight at 20°C, in the presence of 20 mM sodium phosphate buffer at pH 4.5, 6.0, 7.6, 8.4, 9.0, 10.0 and 11.0. These different pH values were tested in order to determine the pH dependence of the I-domain's stability to unfolding. The CD signal was read at 220 nm and averaged for 20 scans per sample with a slit width of 3.0 nm in a 1.0 mm pathlength cell. All samples were monitored with an Applied Photophysics (Leatherhead, Surrey, UK) Pi-Star 180 Circular Dichroism spectrapolarimeter. ΔG_{spec} values were calculated using a non-linear least-squares fit (Equation 9) of the CD titration curves in the program Kaleidagraph.

Melting Transition

H305A and D302A I-domain solutions were diluted to a final concentration of 0.4 mg/mL in the presence of 20 mM sodium phosphate buffer at 7.6. Samples were ramped from 20 to 70 °C, in the case of D302A just 60 °C. At each 0.5 °C increment the CD signal was read at 220 nm with a slit width of 3.0 nm in a 1.0 mm pathlength cell. All samples were monitored with an Applied Photophysics (Leatherhead, Surrey, UK) Pi-Star 180 Circular Dichroism spectrapolarimeter. Melting temperatures were calculated using a non-linear least-squares fit (Equation 10) (Kaleidagraph).

Table of Figures

Figure 1: The assembly pathway of bacteriophage P22 2
Figure 2: CryoEM reconstruction of P22 bacteriophage virion 2
Figure 3: HK97 coat protein structure (A) and P22 coat protein structure (B) in comparison 5
Figure 4: Comparison of the cryoEM models from Parent et al. (2010) and Chen et al.(2011) 5
Figure 5: High resolution structure of the I-domain of bacteriophage P22 6
Figure 6: Structure of the I-domain of P22 with highlighted acidic residues 8
Figure 7: Schematic illustration of 3D ^{1}H-^{15}N NOESY-HSQC 9
Figure 8: Representative pH titration data showing residues Aspartate at position 246 and 317 10
Figure 9: Thermodynamic linkage analysis 13
Figure 10: pH titration of His_6-tag and H305 from WT I-domain from bacteriophage P22 15
Figure 11 High resolution NMR structure of the P22 I-domain 16
Figure 12: Wavelength scans at differerent pH values for WT, H305A and D302A I-domain 20
Figure 13: WT I-domain ΔG_0 values obtained from CD experiments as a function of pH 21
Figure 14: Overlay of WT, H305A and D302A I-domain ΔG_o values obtained from Circular Dichroism experiments as a function of pH dependence 22
Figure 15: Representative equilibrium unfolding urea titration at pH 6.0 23
Figure 16: Comparison of melting transition of WT, H305A and D302A I-domain 25
Figure 17: Schematic illustration of hydrogen-deuterium exchange 26
Figure 18: Overlay of WT I-domain spectrum (blue) and H305A (green) 28
Figure 19: Overlay of WT I-domain spectrum (blue) and D302A (red) 29
Figure 20: Structural mapping of shifting residues in WT and H305A and D302A spectra 30
Figure 21:Representative spectra of Hydrogen Exchange in H305A and D302A I-domain 32
Figure 22: Representative data for exponential decay of ^{1}H-^{15}N crosspeak intensities 33
Figure 23: Sequence dependence of thermodynamic free energy change from HX experiments 34
Figure 24: Structural mapping of $\Delta G_{0,\,HX}$ values 35

Bibliography

1. Teschke, C. M.; Parent, K. N.;. (2010). "Let the phage do the work': using the phage P22 coat protein structures as a framework to understand its folding and assembly mutants. Virology, 401, 119-130.

2. King, J.; Botstein, D.; Casjens, S.; Earnshaw, W.; Harrison, S.; Lenk, E.;. (1976). Structure and assembly of the capsid of bacteriophage P22. 276(37-49).

3. Parent, K. N.; Khayat, R.; Tu, L. H.; Suhanovsky, M. M.; Cortines, J. R.; Teschke, C. M.; Johnson, J. E.; Baker, T. S.;. (2010). P22 Coat Protein Structures Reveal a Novel Mechanism for Capsid Maturation: Stability without Auxiliary Proteins or Chemical Crosslinks. Structure, 18, 390-401.

4. Bazinet, C.; Benbaset, J.; King, J.; Carazo, J. M.; Carrascosa, J. L. (1988). Purification and organization of the gene 1 portal protein required for phage P22 DNA packaging. Biochemistry, 27, 1849-1856.

5. Prasad, B. V. V.; Prevelige, P. E. Jr.; Marieta, E.; Chen, R. O.; Thomas, D.; King, J.; Chiu, W.;. (1993). Three-dimensional transformation of capsids associated with genome packaging in a bacterial virus. J. Mol. Biol., 231, 65-74.

6. Lander, G. C.; Khayat, R.; Li, R.; Prevelige, P. J.; Potter, C. S.; Carragher, B.; Johnson, J. E.;. (2009). The P22 tail machine at subnanometer resolution reveals the architechture of an infectious conduit. 17, 789-799.

7. Baker, M. L.; Jiang, W.; Rixon, F. J.; Chiu, W. (2005). Common Ancestry of Herpesviruses and Tailed DNA Bacteriophages. Journal of Virology, 79, 14967-14970.

8. Johnson, J. E.; Chiu, W.;. (2007). DNA packaging and delivery machines in tailed bacteriophages. Current Opinion in Structural Biology, 17, 237-243.

9. Wikoff, W. R.; Liljas, L.; Duda, R. L.; Tsuruta, H.; Hendrix, R. W.; Johnson, J. E.;. (2000, September 22). Topologically linked protein rings in the bacteriophage HK97 capsid. Science, 289, 2129-2133.

10. Lander, G. C.; Tang, L.; Casjens, S. R.; Gilcrease, E. B.; Prevelige, P.; Poliakov, A.; Potter, C. S.; Carragher, B.; Johnson, J. E.;. (2006). The Structure of an Infectious P22 Virion Shows the Signal for Headful DNA Packaging. Science, 312, 1791-1795.

11. Suhanovsky, M. M.; Teschke, C. M.;. (2013). An Intramolecular Chaperone Inserted in Bacteriophage P22 Coat Protein Mediates Its Chaperonin-independent Folding. The Journal of Biological Chemistry, 288, 33772-33783.

12. Chen, D. H.; Baker, M. L.; Hryc, C. F.; DiMaio, F.; Jakana, J.; Wu, W.; Dougherty, M.; Haase-Pettingell, C.; Schmid, M. F.; Jiang, W.; Baker, D.; King, J. A.; Chiu, W.;. (2011). Structural basis for scaffolding-mediated assembly and maturation of a dsDNA virus. Proceedings of the National Academy of Sciences of the United States of America, 108, 1355-1360.

13. Rizzo, A. A.; Suhanovsky, M. M.; Baker, M. L.; Fraser, L. C. R.; Jones, L. M.; Rempel, D. L.; Gross, M. L.; Chiu, W.; Alexandrescu, A. T.; Teschke, C. M.;. (2014). Multiple Functional Roles of the Accessory I-Domain of Bacteriophage P22 Coat Protein Revealed by NMR Structure and CryoEM Modeling. Structure, 22, 830-841.

14. Gordon, C. L.; King, J.;. (1993). Temperature-sensitive mutations in the phage P22 coat protein which interfere with polypeptide chain folding. Journal of Biological Chemistry, 268, 9358-9368.

15. Teschke, C. M.;. (1999). Aggregation and Assembly of Phage P22 Temperature-Sensitive Coat Protein Mutants in Vitro Mimic the in Vivo Phenotype. Biochemistry, 38, 2873-2881.

16. Nakonechny, W. S.; Teschke, C. M.;. (1998). GroEL and GroES control of substrate flux in the in vivo folding pathway of phage P22 coat protein. The Journal of Biological Chemistry, 273, 27236-27244.

17. Singer, A. U.; Forman-Kay, J. D.;. (1997). pH Titration studies of an SH2 domain phosphopeptide complex: Unusual histidine and phosphate pKa values. Protein Science, 6, 1910-1919.

18. Sheftic, S. R.; Croke, R. L.; LaRochelle, J. R.; Alexandrescu, A. T.;. (2009). Electrostatic Contributions to the Stabilities of Native Proteins and Amyloid Complexes. Methods in Enzymology, 466, 233-259.

19. Markley, J. L.;. (1975). Mutual electrostatic interaction between histidine residues 12 and 119. Biochemistry, 14, 3562—3566.

20. Sachs, D. H.; Schechter, A. N.; Cohen, J. S.;. (1971). Nuclear Magnetic Resonance Titration Curves of Histidine Ring Protons. The Journal of Biological Chemistry, 246, 6576-6580.

21. Wuthrich, K.;. (1986). NMR of Proteins and Nucleic Acids.

22. Thurkill, R. L.; Grimsley, G. R.; Scholtz, J. M.; Pace, C. M.;. (2006). pk values of the ionizable groups of proteins. Protein Science, 15, 1214-1218.

23. Pace, C. N.;. (1986). Determination and Analysis of Urea and Guanidine Hydrochloride Denaturation Curves. Methods in Enzymology, 131, 266-280.

24. Santoro, M. M.; Bolen, D. W.;. (1988, June 2). Unfolding Free Energy Changes Determined by the Linear Extrapolation Method. 1. Unfolding of Phenylmethanesulfonyl alpha-Chymotrypsin Using Different Denaturants. Biochemistry, 27, 8063-8068.

25. Kuhlmann, B.; Boice, J. A.; Fairman, R.; Raleigh, D. P.;. (1998). Structure and Stability of the N-Terminal Domain of the Ribosomal Protein L9: Evidence for Rapid Two-State Folding. Biochemistry, 37, 1025-1032.

26. Wagner, G.; Wuthrich, K.;. (1979). Structural Interpretation of the Amide Proton Exchange in the Basic Pancreatic Trypsin Inhibitor and Related Proteins. Journal of Molecular Biology, 134, 75-94.

27. Hoofnagle, A. N.; Resing, K. A.; Ahn, N. G. (2003). Protein Analysis by Hydrogen Exchange Mass Spectrometry. Annual Review of Biophysics and Biomolecular Structure, 32, 1-25.

28. Bai, Y.; Milne, J. S.; Mayne, L.; Englander, S. W. (1994). Protein Stability Parameters Measured by Hydrogen Exchange. Proteins, 20, 4-14.

29. Alexandrescu, A. T.; Jaravine, V. A.; Dames, S. A.; Lamour, F. P. (1999). NMR Hydrogen Exchange of the OB-fold Protein LysN as a function of Denaturant: The Most Conserved Elements of Structure are the Most Stable to Unfolding. Journal of Molecular Biology, 289, 1041-1054.

30. Bai, J.; Milne, J. S.; Mayne, L.; Englander, S. W. (1993). Primary Structure Effects on Peptide Group Hydrogen Exchange. Proteins: Struct. Funct. Genet., 17, 75-86.

31. Zhang, Y. Z.;. (1995). Protein and peptide structure and interactions studied by hydrogen exchange and NMR. Structural Biology and Molecular Biophysics, University of Pennsylvania, PA, USA.